

UC San Diego

UC San Diego Electronic Theses and Dissertations

Title

Design and analysis of a kirigami-based two-finger microgripper

Permalink

<https://escholarship.org/uc/item/98t1b6zk>

Author

Mondal, Sayan

Publication Date

2020

Peer reviewed|Thesis/dissertation

UNIVERSITY OF CALIFORNIA SAN DIEGO

Design and analysis of a kirigami-based two-finger microgripper

A thesis submitted in partial satisfaction of the
requirements for the degree
Master of Science

in

Engineering Sciences (Mechanical Engineering)

by

Sayan Mondal

Committee in charge:

Professor Nicholas G. Gravish, Chair
Professor Tania Morimoto
Professor Michael T. Tolley

2020

Copyright
Sayan Mondal, 2020
All rights reserved.

The thesis of Sayan Mondal is approved, and it is acceptable in quality and form for publication on microfilm and electronically:

Chair

University of California San Diego

2020

DEDICATION

To my parents: Jitendra Narayan Mondal and Sarmistha Mondal.

EPIGRAPH

*Knowledge can only be got in
one way, the way of experience;
there is no other way to know.*

—Swami Vivekananda

TABLE OF CONTENTS

Signature Page	iii
Dedication	iv
Epigraph	v
Table of Contents	vi
List of Figures	viii
List of Tables	x
Acknowledgements	xi
Vita	xii
Abstract of the Thesis	xiii
Chapter 1	Introduction	1
	1.1 Background	1
	1.2 Motivation	2
	1.3 Related Works	5
	1.4 Overview of the Master’s Thesis	6
Chapter 2	Design and Fabrication	7
	2.1 Background	7
	2.2 Working principle of the gripper	8
	2.3 Microgripper fabrication details	9
	2.4 Challenges associated with the design	12
Chapter 3	Kinematic Analysis	14
	3.1 Background	14
	3.2 Relationship between Input Angle and Output Angle	15
	3.2.1 Design parameters	15
	3.2.2 Homogeneous Transformations	17
	3.3 Workspace of the microgripper	22
	3.4 Experiments and Results	24
	3.5 Kinematic Ratio of the microgripper	27
	3.6 Influence due to the various Design Parameter	28
	3.7 Configuration Space of the microgripper: A case study	32

Chapter 4	Static Analysis	35
	4.1 Background	35
	4.2 Flexure Stiffness of the hinge joints	35
	4.3 Actuation Force	36
	4.4 Grasping Force	39
	4.5 Mechanical Advantage of the microgripper	41
	4.6 Static Analysis on the hexagonal nut	42
	4.6.1 Gripper Modifications	44
Chapter 5	Conclusion and Future Work	51
Bibliography	55

LIST OF FIGURES

Figure 1.1:	A wide range of grippers.	2
Figure 1.2:	A colony of ants: nature’s swarm robots.	3
Figure 1.4:	A flow diagram showing the different components of the project.	5
Figure 1.5:	The part of the project that we focused here.	5
Figure 2.1:	Schematic diagram highlighting the links and joints of the gripper design	8
Figure 2.2:	The fundamental concept on which the gripper’s working principle is based.	9
Figure 2.3:	Design flow of the microgripper.	10
Figure 2.5:	Laminated layers of the microgripper ready for release cut.	12
Figure 2.6:	A schematic diagram of a slot-joint pair (exxagerated) and a simple fix to make it easier to insert the joint into the slot.	13
Figure 3.1:	Schematic diagrams highlighting the Input Angle, θ and the Output Angle, ϕ of the gripper.	15
Figure 3.2:	The top view and the side view of the gripper, showing the design parameters.	16
Figure 3.3:	Defining the end points of the tendon.	17
Figure 3.4:	The top view and the side view of the gripper, showing the transformation axes.	18
Figure 3.5:	The plot showing the relationship between the input angle and the output angle.	21
Figure 3.6:	The top view of the gripper, showing the jaw opening.	22
Figure 3.7:	Jaw Path Profile w.r.t axis-2.	23
Figure 3.8:	Experimental Setup.	24
Figure 3.9:	Samples from the experiment	25
Figure 3.10:	Experimental Validation.	26
Figure 3.11:	Simulation in MathWorks Simscape.	26
Figure 3.12:	Simulation Validation.	27
Figure 3.13:	Kinematic Ratio of the gripper	28
Figure 3.14:	Influence of the Design Parameters on Output Angle.	29
Figure 3.15:	Influence of the Design Parameters on Jaw Opening.	30
Figure 3.16:	Specifications of some of the target objects for grasping.	32
Figure 4.1:	Input force required to actuate the gripper.	37
Figure 4.2:	Actuation force plot	38
Figure 4.3:	Gripping Contact Force of the gripper.	39
Figure 4.4:	Output force plot	40
Figure 4.5:	Actuator force and Output force.	41
Figure 4.6:	Mechanical Advantage of the gripper	42
Figure 4.7:	A simple experiment demonstrating the elasticity in a kirigami structure.	44
Figure 4.8:	An image of the kirigami spring in action.	45
Figure 4.9:	Modeling kirigami spring that has been incorporated in the new design.	46
Figure 4.10:	Influence of Kirigami spring on output force and on actuator force.	48

Figure 4.11: Images showing grasping of the target objects.	48
Figure 4.12: Some of the final images of the gripper.	49
Figure 4.13: Influence of input hinge length on actuator force.	50
Figure 5.1: Some kirigami test patterns.	52

LIST OF TABLES

Table 3.1: Summary of the influence of the various design parameters on the output angle and jaw opening.	28
---	----

ACKNOWLEDGEMENTS

I wish to extend my sincerest gratitude to my advisor, Dr. Nicholas G. Gravish for his help and guidance towards the work contained in this thesis. I have learnt a tremendous amount through the discussions that we have had together. This thesis would not have been what it is without him.

I am very grateful to the rest of the members of my committee namely, Dr. Michael T. Tolley and Dr. Tania Morimoto for their time and support.

I am eternally grateful to my parents, my elder sister for their constant motivation and unwavering faith in me. Their love and encouragement has been critical for the successful completion of my degree.

This thesis is currently being prepared for submission for publication of the material. Mondal, Sayan - The thesis author was the primary investigator and author of this material.

VITA

2016 B. E. in Mechanical Engineering, Jadavpur University, Kolkata, India
2018-2019 Graduate Teaching Assistant, University of California, San Diego
2020 Master of Science in Mechanical Engineering, University of California, San Diego

PUBLICATIONS

Anwesan Pal, **Sayan Mondal**, Henrik I. Christensen, "Looking at the right stuff"- Guided semantic-gaze for autonomous driving, *IEEE/CVF Conference on Computer Vision and Pattern Recognition, 2020*.

ABSTRACT OF THE THESIS

Design and analysis of a kirigami-based two-finger microgripper

by

Sayan Mondal

Master of Science in Engineering Sciences (Mechanical Engineering)

University of California San Diego, 2020

Professor Nicholas G. Gravish, Chair

This masters thesis describes a novel underactuated robotic microgripper with two fingers. The design specifications, a thorough kinematic description of the gripper, and its static analysis are presented. The novelty of this gripper lies in the simplicity of its mechanism that can accomplish the task of picking up the target objects. What makes it unique is its ability to grasp objects that are either in the same plane as that of the gripper or are at a lower level. The gripper is equipped to be actuated by a single actuator. For preliminary evaluation of the gripper's object manipulation capabilities, standard hexagonal nuts with varying weights, and sizes were selected. The success of grasping the nuts by the gripper at two different orientations were observed and studied. In this paper only one of the test cases has been shown in detail. In addition to that, a

kirigami spring has been incorporated in the modified design of the gripper in order to enhance its grasping capabilities.

Chapter 1

Introduction

1.1 Background

All species in the animal kingdom can effectively manipulate objects of various geometries (shapes and sizes), weights, and materials using a variety of action modes such as grasping, pushing, sliding, tipping, rolling, and throwing. Most manipulation action modes mentioned above are highly sensitive to uncertainties associated to object's state, geometry, mass, friction, and restitution, and to the robot's own control errors. In contrast, most robots manipulate objects by pick-and-place. It is because once a firm grasp has been established, the robot can reliably control the motion of the object without needing to continuously sense the state of the object or correct for modeling uncertainties. However, restricting robotic manipulators to only grasp objects limits the set of tasks that they can accomplish. Nonetheless, the pick-and-place task which appears to be relatively simple, has its own set of challenges and its performance is greatly dependent on the design of the manipulator itself. The design of the gripper is one of the crucial deciding factors on how well the robot would be able to manipulate objects. Without an appropriate design, it will inevitably fail to accomplish the task of manipulation, even if the robot is equipped with the best sensors, the perfect controllers and is embedded with the state-of-the-art

planning algorithms. In this thesis we will discuss about a novel gripper mechanism and will mainly focus on the design and analysis aspect of it.

1.2 Motivation

There are grippers all around us and they come in various forms. They range from a trash grabber to an industrial robot arm. Even a flexible tripod can be imagined to be a gripper that can hold on to some fixed support. This displays the broad range of applications



Figure 1.1: A wide range of grippers.

of grippers. There is also a special group of grippers that draw their inspiration from biology. To expand more on bioinspired grippers we have illustrated a few examples. There are soft grippers made up of fluidic elastomers along with gecko-inspired adhesive [GSR⁺18] in order to enhance their grasping capabilities. They have applications in industrial automation and in-space operations. Another interesting soft gripper has been inspired by the clingfish suction disc [SJQ⁺19]. It allows reversible adhesion to rough surfaces both in and out of water and thus is suitable for underwater exploration. They are also known for handling delicate objects. There are tetherless thermobiochemically actuated microgrippers [LRB⁺09] whose design is inspired by the dicondylic joints of arthropods. They are even inspired by the biological function in nature that is often achieved by autonomous organisms and cellular components when triggered en

masse by relatively benign cues, such as small temperature changes and biochemicals. There are also mechanical surgical snake robots [HSB19] that are designed to perform minimally invasive surgeries like laparoscopy or removal of tumours in the brain. In this case the robot itself is bioinspired and the end-effector is designed so that it is compatible with the design of the robot. These shows that based on the complexity of the task and the nature of the working environment, certain useful features from biology are engineered so as to mimic similar or even superior characteristics in robots or tools.

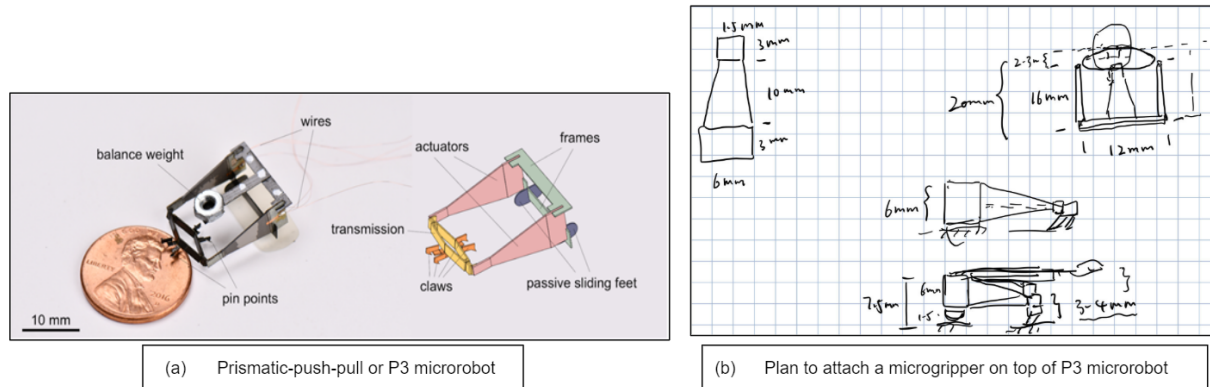
There is another area in robotics known as swarm robotics that largely draws inspirations from biology or nature. Just like a colony of ants work together to accomplish some big task like building their nests, in swarm robotics, simple robots are designed so as to perform complex tasks more efficiently by working together as compared to expensive large complicated robots. Thus there is a demand to build simple robots that are cost-efficient and are mass producible in a short period of time. In our laboratory (Gravish Lab) we are motivated to achieve the first step



Figure 1.2: A colony of ants: nature's swarm robots.

of the task where a simple cost-efficient mobile robot is capable of capturing and retrieving of objects from hard-to-reach places. A simple microrobot known as prismatic-push-pull or P3 robot [ZG20] has been developed in our laboratory. It is shown in the figure 1.3(a).

The microrobot has claws that are connected to the piezoelectric actuators on its sides through a transmission. The actuation results in back and forth motion of the claws which causes the robot to move forward. We came up with the idea of designing a microgripper for P3 robot which will be capable of picking small objects as exhibited in a schematic diagram in figure 1.4. Together



(a) Prismatic-push-pull or P3 microrobot

(b) Plan to attach a microgripper on top of P3 microrobot

Figure 1.3: Early stage of the idea on development of a gripper for the P3 robot *

they can accomplish a task such as navigating to a location under a cabinet, that is out-of-reach for human hand, picking up an object such as a small hexagonal nut, and carrying the object out of that place, before finally releasing it. To achieve this we first looked into the dimensions of the P3 robot. We measured the area of the space available on P3 robot. This is the area within which the microgripper needs to fit. It is measured to be around $12\text{ mm} \times 20\text{ mm}$ (refer fig.1.3(b)). We also noted that the base of the gripper will be around 7.5 mm from the ground since it is going to be attached on the top of the P3 robot. Other important dimensions for our gripper design was the tip of the PZT actuator. Our initial plan was to design a gripper that could be actuated with the same kind of actuators that are used in the P3 robot. This would mean that we do not have to invest any additional time for the design of the actuator specific to our microgripper. Thus the actuators tip area, which is $1.5\text{ mm} \times 3\text{ mm}$, was taken into account in the gripper design. With miniaturization it becomes difficult to accommodate more number of actuators and sensors. Thus we demanded of a microgripper that will be actuated by a single actuator and can bend and open its jaws so as to pick small objects from the ground. Our work here focuses on the design part of the microgripper (fig.1.5) for P3 like microrobots.

*The image (a) is taken from [ZG20]

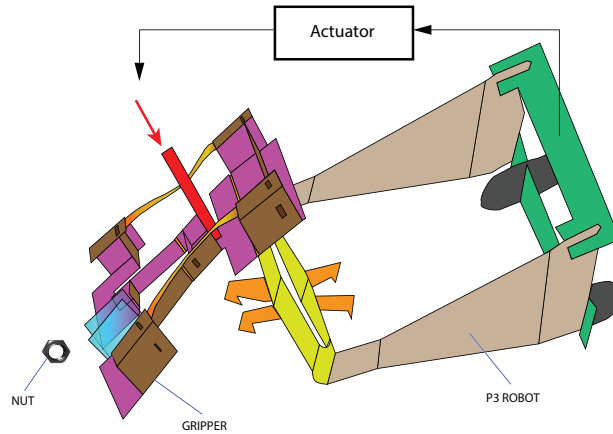


Figure 1.4: A flow diagram showing the different components of the project.

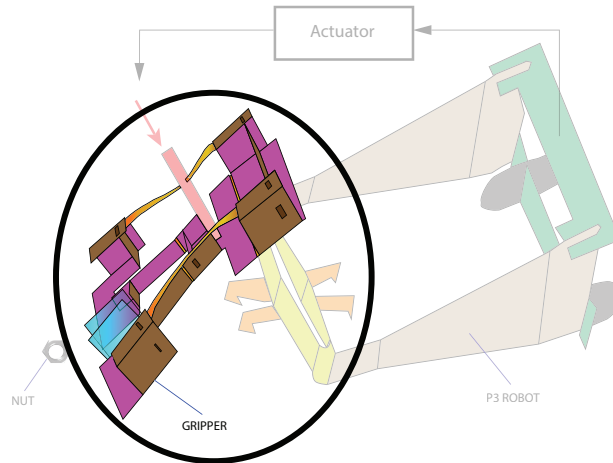


Figure 1.5: The part of the project that we focused here.

1.3 Related Works

We looked into some of the existing microgrippers to find if there is any such gripper that meets our requirements. Some of the advanced microgrippers such as a silicon-processed overhanging microgripper [KPM92], a polysilicon, electrostatic, comb-drive microgripper [KPML90], SMA microgripper system [KKJ02], compliant microgripper system [WLT⁺16, NZ07], and high precision flexure-based microgripper [ZS09] have the great potential for handling micro-objects with high precision. However, these microgrippers are capable of grasping the objects only when they are placed in the same plane as that of the gripper. The

microgrippers are mostly categorised based on the type of actuators used.

There is another very interesting type of microgrippers developed. They are capable of self-folding [BYX⁺15], are tetherless [LRB⁺09] and can be used to pick-and-place micro objects [RLB⁺08]. They are shown to have microsurgical applications. However, we notice that there is a need of an external magnetic source in order to navigate and control them. Also, the closing of these microgrippers is triggered by some thermochemical reaction in an aqueous solution. This happens due to the release of the residual stresses at the joints. These mobile microgrippers are thus unsuitable for our application. We needed a microgripper that can navigate on land and is capable of picking up small objects.

1.4 Overview of the Master's Thesis

Chapter 2, presents the process involved in the design and fabrication of the microgripper.

Chapter 3 provides an in-depth kinematic analysis of the gripper and highlights the influence of the various design parameters in regard to the kinematics of the gripper. There is case study done on the success of grasping of a hexagonal nut, which is the target object chosen for our microgripper.

Chapter 4 deals with the static analysis of the gripper. It also discusses some of the drawbacks of the gripper and suggests the remedies to fix them. The case study on the target hexagonal nut is continued in this chapter, and here we study the statics component of it.

Chapter 5, which is the last chapter, we draw the conclusions regarding our microgripper design. Here we also suggest the future work that needs to be done in order to overcome some of the difficulties faced by us in designing the gripper. In future work we also mentioned a few potential actuators that can be used for our microgripper.

Chapter 2

Design and Fabrication

2.1 Background

As mentioned in the paper [WAS⁺08], mobile microrobots with characteristic dimensions in the order of 1cm are difficult to design using either MEMS (micromechanical systems) technology or precision machining. In the creation of our microgripper we have used the Smart Composite Microstructures (SCM) framework as introduced in that paper. This design approach guarantees the creation of the microgripper to be robust and can be rapidly prototyped. These are important design factors to be considered, as in swarm-robotics we desire to produce a large number of robots in a limited amount of time at a reasonably low cost. Some of the advantages of micromechanical systems involves higher accuracy, and gentleness [Tri89]. This comes at a price of unconventional design procedures as at that scale almost no component is readily available in the market.

2.2 Working principle of the gripper

The gripper comprises of three linkages and three revolute joints as shown in the figure 2.1. The revolute joint connecting the base link-1 to link-2 is the *input* hinge/flexural joint. The other two identical revolute joints connecting link-2 to each of the linkages-3 (that comprises of one of the gripper's end-effectors, namely the left jaw and the right jaw), are the *output* hinge/flexural joints.

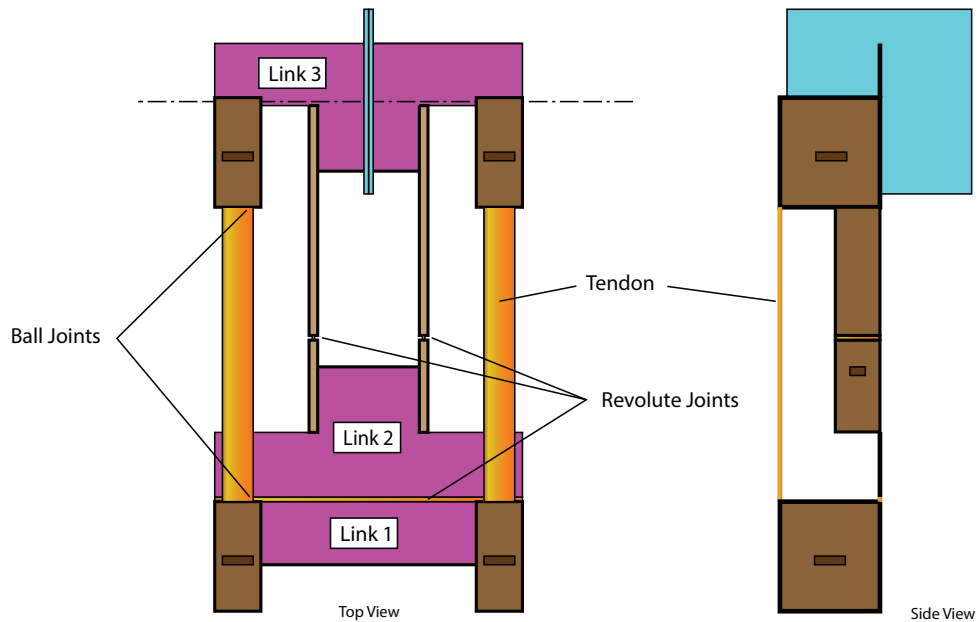


Figure 2.1: Schematic diagram highlighting the links and joints of the gripper design

The input and the output joints are orthogonal to each other, i.e. their axes of rotation are perpendicular for all gripper states. Linkages-3 are connected to link-1 with the help of a tendons. The tendons are assumed to be inextensible and they cannot resist any compressive forces. The tendons thus serve the purpose of imposing a constant-distance constraint between the two connecting linkages. There is an offset distance between the plane that consists of the input joint and the plane where the tendons lie. This offset distance is the main crux behind the functioning of the gripper. As we know during bending of a beam the fibers at concave side undergoes maximum compression and the fibers at the convex side experiences maximum tension

(see fig. 2.2). Here the main takeaway is the tension increases with the increase of distance between the neutral plane and the fibers at the convex end. Similarly, when the gripper is actuated, i.e. when the link-2 is bent about the input hinge joint, there is a tension generated at the tendons due to the offset distance. Due to the tension at the tendons there is a moment generated about the output hinge joints that causes the gripper jaws to open.

Thus we see that the microgripper has a tendency to return back to its original unactuated configuration upon withdrawal of the external force. This is because of the restoring torques generated at the hinge joints due to bending. This makes the grasping and lifting mode passive and it requires no power to actuate the gripper once it successfully grasps the target object.

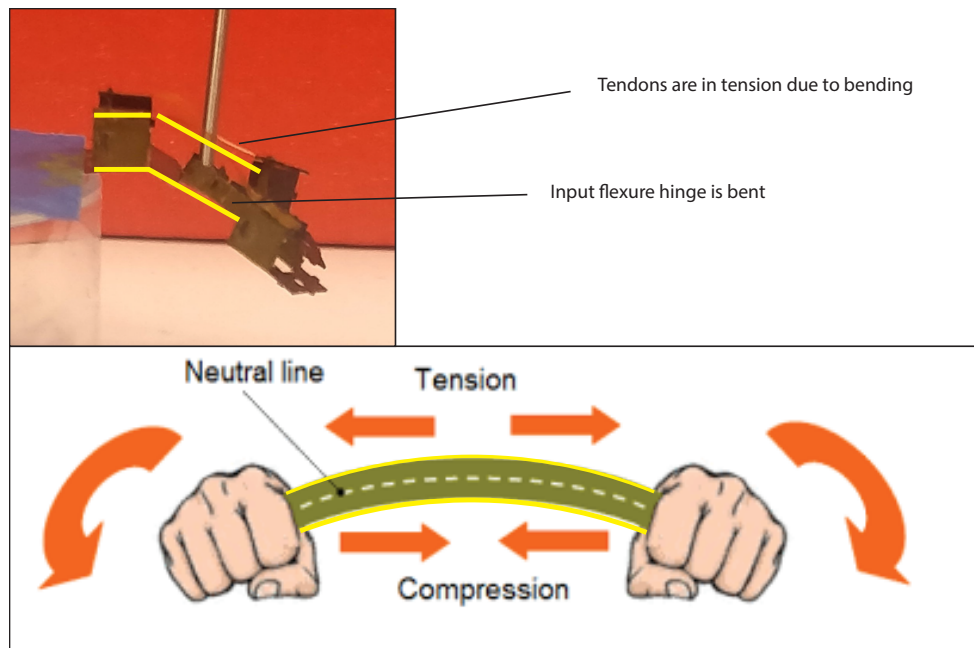


Figure 2.2: The fundamental concept on which the gripper's working principle is based.

2.3 Microgripper fabrication details

The microgripper is made out of 80 microns carbon fiber 0° - 90° - 0° composite that acts as a rigid material, a DuPont 300HN Kapton polymer layer that provides compliance to the design

and a thermal-adhesive layer for binding the carbon fiber composite with the kapton layer. The entire microgripper is designed out of 21 mm×21 mm area of the above mentioned layers.

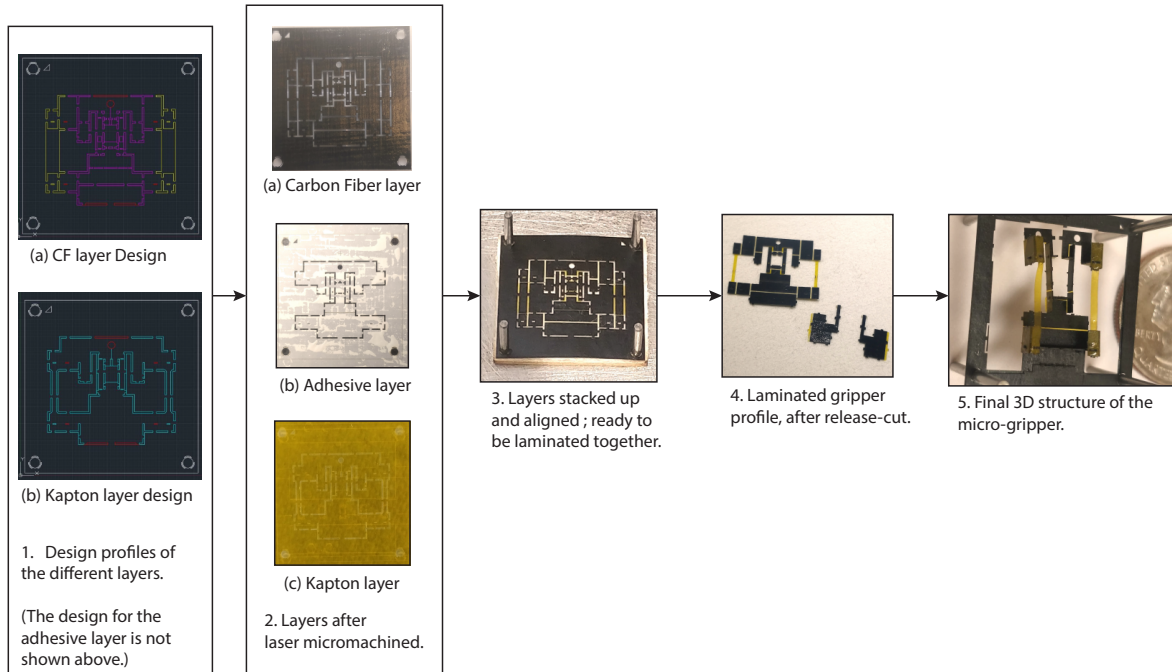


Figure 2.3: Design flow of the microgripper.

The entire design flow of the gripper is shown in the figure 2.3. The fabrication process consists of laser micromachining the rigid composite carbon fiber layer and the kapton polymer layer to achieve a desired compliance profile. The links are created when kapton layer is stacked with the carbon fiber layer. The gaps in the carbon fiber layer where there is only the kapton polymer present create the flexures, which either acts as hinge joints or allow folding of the composite laminate so as to achieve the final 3D structure of the microgripper.

For the rotational flexural design, unlike sandwiching the polymer in between two composites as suggested in the paper [WAS⁺08], in our microgripper fabrication, there is composite carbon fiber layer only on one side of the kapton (see fig.2.4). The reason for having this difference is we wanted to test the mechanism of the gripper and thus kept the fabrication process simple. Later on another carbon fiber layer can be easily added in order to prevent failures such as

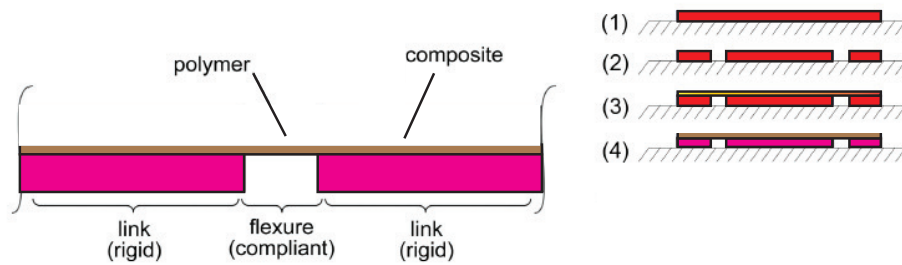


Figure 2.4: Rotational flexure mechanism and associated process *

peeling between the carbon fiber and the kapton layers or propagation of cracks in the kapton layer. Another reason why we did not sandwich the kapton layers in between two carbon fiber layers is that in our gripper mechanism there is only uni-directional bending involved about all the hinges. The gaps for the hinge joints were chosen to be 0.15 mm and those for folding were 0.50 mm . Once the laser micromachining is complete, the next step is to align the carbon fiber layer design profile with that of the kapton. In between the two layers is the lasercut thermal-adhesive layer that helps in the adhering of the two layers on application of heat. Once the layers are aligned the next step is the lamination step. The cure cycle reaches a maximum temperature of 177°C and is maintained for 4 hours . During this step a pressure of around 400 psi was applied using a hydraulic press in order to obtain a stronger adhesion of the layers. After the lamination step, the laminated layer is allowed to cool down to the room temperature, before it is ready for the release cut. Finally, after release cutting the laminated piece (figure 2.5) and removing the extra materials, it is folded manually and the final 3D structure of the gripper is obtained. There are a couple of slot-joints that help to retain the 3D configuration of the gripper. Then we glue all the slot-joints permanently (see fig. 2.6).

*This image has been taken and modified from [WAS⁺08]

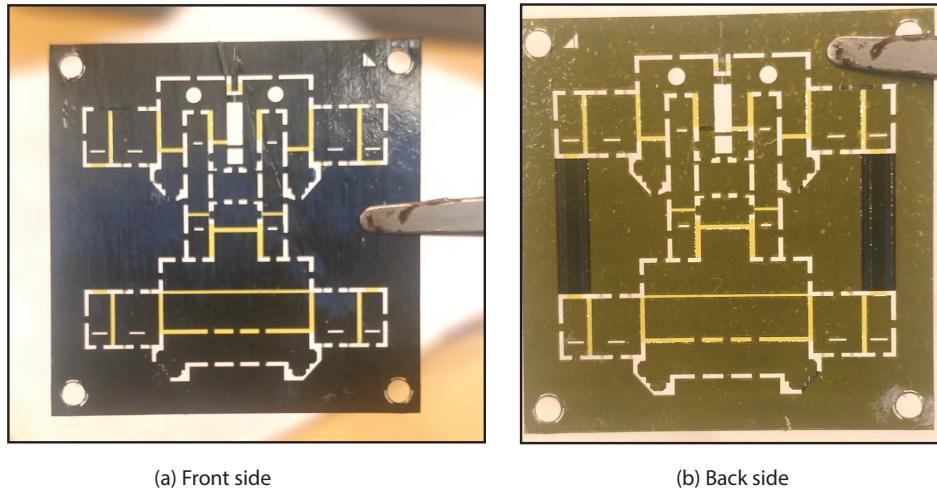


Figure 2.5: Laminated layers of the microgripper ready for release cut.

2.4 Challenges associated with the design

As mentioned earlier grasping in itself is a difficult task to accomplish, but the difficulty level increases by many folds when dealing with micro-robotics due to the challenges associated with miniaturization. The centimeter- and millimeter-sized available mechanical and electronic systems become very difficult to build for the scaled-down versions in the micro domain [Tri89]. An approach suggested in this paper is to first build the necessary actuators and sensors and then integrate these into the micro systems.

Here are some the major challenges that were involved in creating the microgripper:

1. There is complexity associated with the design process. Due to this it needs a rigorous amount of planning. All the three layers, namely carbon fiber, kapton and thermal-adhesive have different design patterns. The planning is necessary as it is required to find the locations where supporting materials needs to be present during the lamination process so that all the layers could be aligned properly without falling apart.
2. The final 3D structure of the gripper involves several 90° folding and additionally, it requires inserting the joints into its slots before finally gluing them. The level of precision involved

with the design of the joint-slots are immense. Otherwise the joints would either not fit into the slots or they would be too loose if the clearance is large. Manually inserting the joints into the slots required a large amount of dexterity and patience. A modified joint design (fig. 2.6) made the process easier without compromising on any additional tolerance in the slot dimensions.

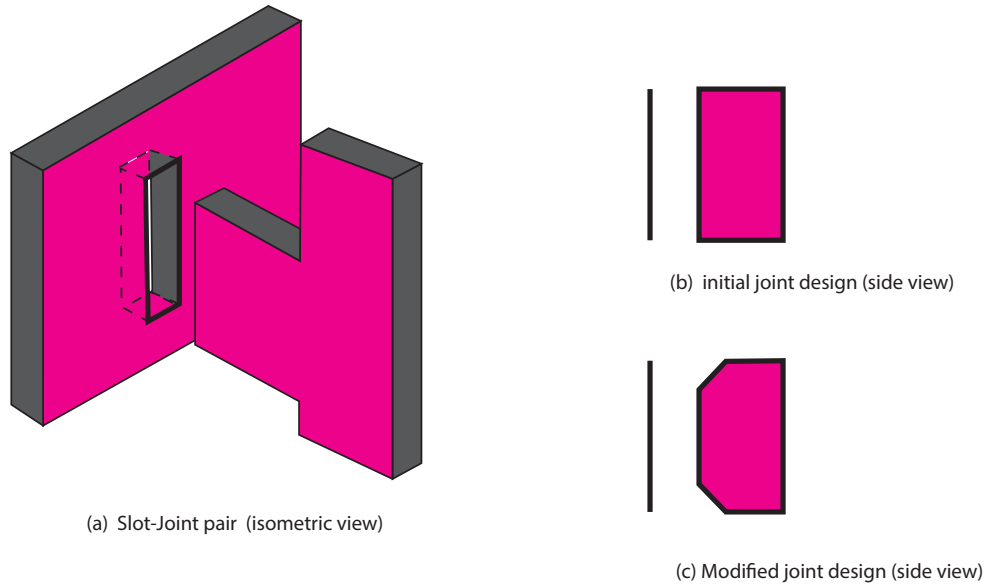


Figure 2.6: A schematic diagram of a slot-joint pair (exaggerated) and a simple fix to make it easier to insert the joint into the slot.

3. Incorporating a kirigami spring in the modified version of the microgripper was quite challenging.

Chapter 3

Kinematic Analysis

3.1 Background

There is no gripper that can grasp objects of any shape and size. Even “human hand”, which is considered to be one of the best known grippers, has its limitations. The geometry of the target object is one of the deciding factors for the design of the gripper.

In this chapter we will find the analytical model of the gripper, i.e. the relationship between the input angle θ and the output angle ϕ (see figure 3.1) , the relationship between the input angle and the jaw opening. We are also going to find the trajectory of the gripper jaw tip which is crucial for knowing what shape and size of objects the particular gripper is capable of making contact with. Making contact with the target objects is the first step towards successfully grasping any object. We have also pointed out the various design parameters that influence the *kinematics* of the gripper and visualize the extent of their influence with the help of plots. These design parameters are necessary but not sufficient, for answering whether a gripper would be successful in accomplishing the task of grasping a target object or not. The other determining design parameters are discussed in the chapter - *Static Analysis*.

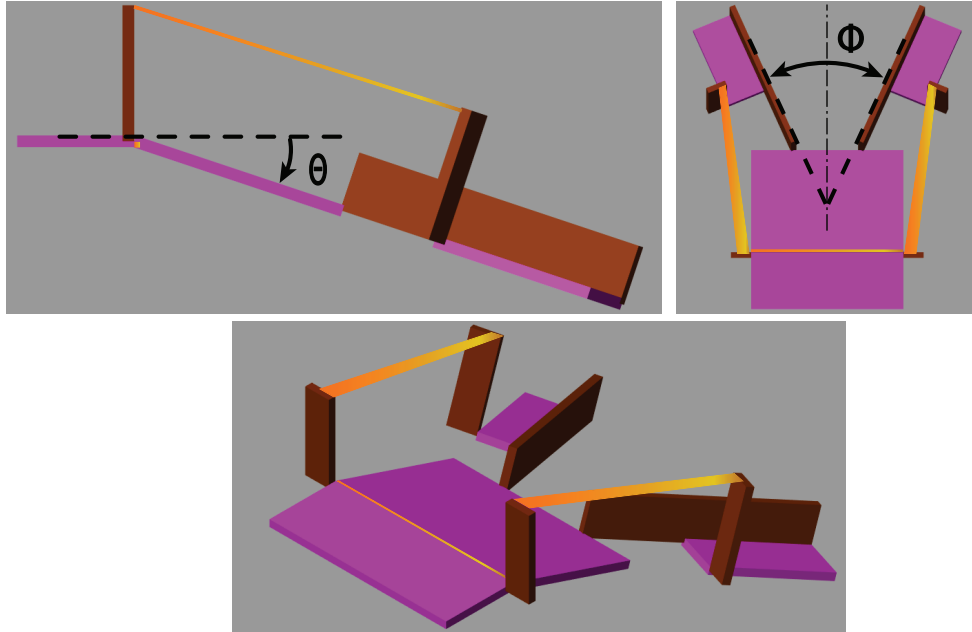


Figure 3.1: Schematic diagrams highlighting the Input Angle, θ and the Output Angle, ϕ of the gripper.

3.2 Relationship between Input Angle and Output Angle

As seen in the previous chapter in the figure 2.1, the gripper can be interpreted as a mechanical system with three rigid links, an input revolute joint and two output revolute joints. There is a constant-distance constraint due to the tendons connecting link-1 with link-3. In this section we will establish the relationship between the input angle θ and the output angle ϕ . The input angle is the angle of rotation about the input hinge and the output angle is the angle of rotation about the output hinge joints as shown in the figure 3.1. In order to do so we first define the various design parameters and then make use of homogeneous matrix transformation in order to find the distance between the end points of the tendon. Finally we apply the constant-distance constraint in order to get the analytical model mapping the input angle to the output angle.

3.2.1 Design parameters

As shown in the figure 3.2, we first define the various design parameters of the gripper.

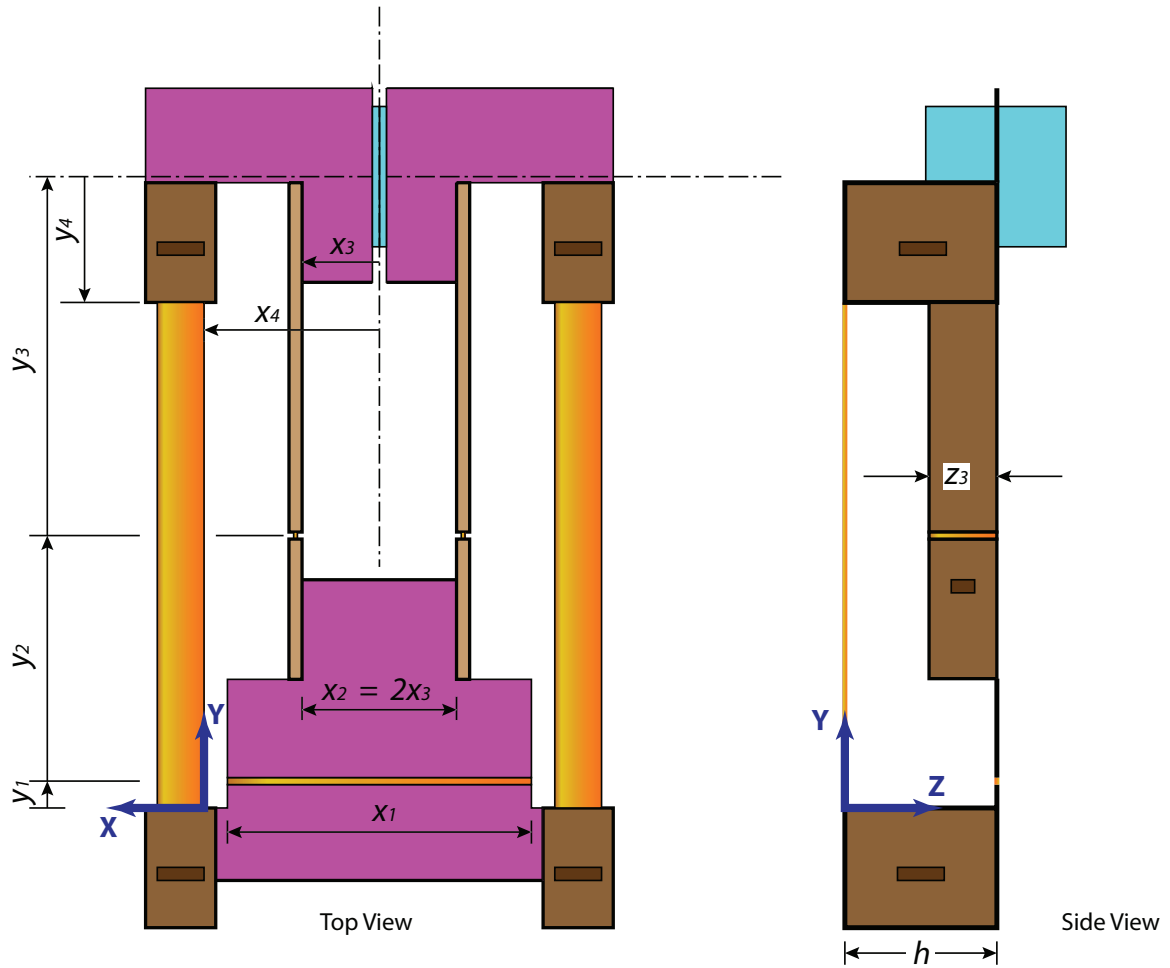


Figure 3.2: The top view and the side view of the gripper, showing the design parameters.

- y_1 : The distance along y -direction between the link-1's point of attachment to the tendon and the input hinge joint.
- y_2 : The distance along y -direction between the input hinge joint and the output hinge joint.
- y_3 : The distance along y -direction between the output hinge joint and the gripper's jaw x -centerline.
- y_4 : The distance along y -direction between the gripper's jaw x -centerline and the link-3's point of attachment to the tendon.
- x_1 : The width of the input hinge joint.

- x_2 : It is the distance between the two output hinge joints.
- x_3 : The distance along x-direction between the gripper's jaw y-centerline and the output hinge.
- x_4 : The distance along x-direction from the gripper's jaw y-centerline to the tendon.
- z_3 : The width of the output hinge joint.
- h : The z-offset of the tendon from the plane containing of the input hinge joint.

Note: x_1 and z_3 are important static analysis design parameters while the rest are important for kinematic analysis of the gripper.

3.2.2 Homogeneous Transformations

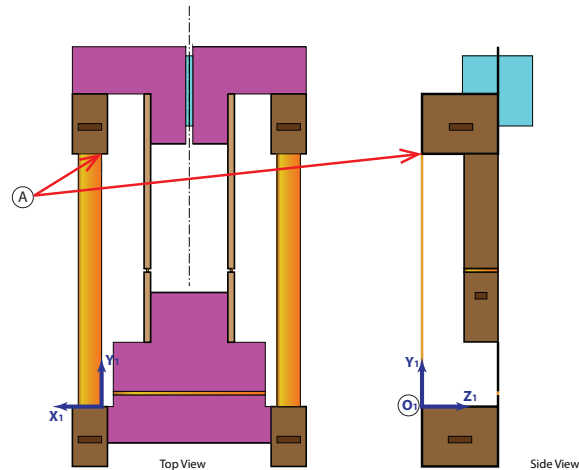


Figure 3.3: Defining the end points of the tendon.

For all states or configuration space of the gripper, i.e. $\forall \theta$, the constant-distance constraint between the two end points, namely O_1 and A will hold true (see figure 3.3). Notice that the points on the tendon are chosen such that they are closest to the the jaw. This is because we achieve the constant-distance constraint with tendons made up of the kapton layer of finite width ($1mm$). The gripper, when bent about the input hinge, causes the innermost filament of the kapton

polymer to experience tension and the outermost filament will experience a slack, resulting in a slight amount of twisting of the tendon.

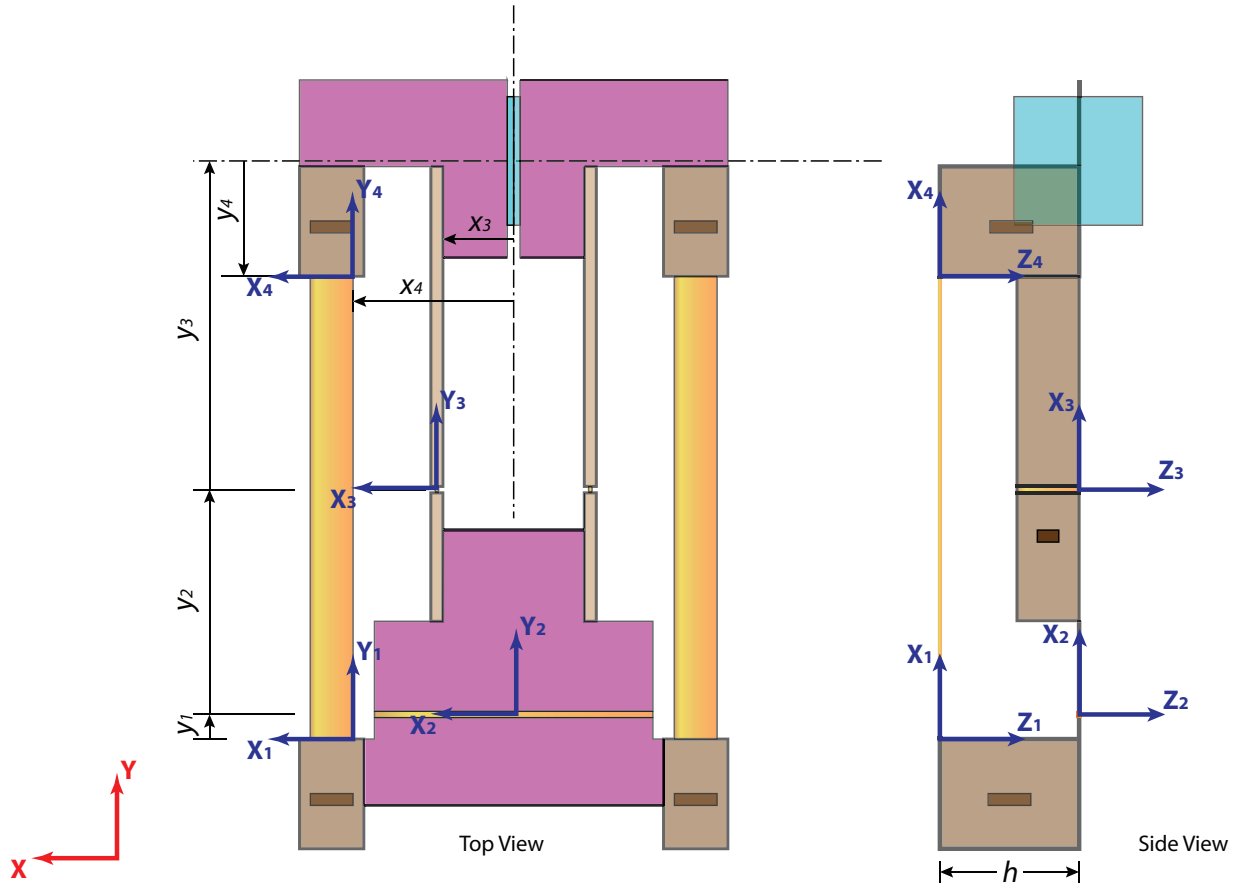


Figure 3.4: The top view and the side view of the gripper, showing the transformation axes.

Next we define a set of local coordinate axes as shown in the figure 3.4. Axis-1 is attached to link-1 at O_1 , axis-2 is attached to link-2 at the input hinge joint, and axes-3 and 4 are attached to link 3 at the base of the output hinge joint and at A respectively. With the help of the defined axes we apply the homogeneous matrix transformations as follows.

$$\mathcal{H}_2^1 = \mathcal{T}_2^1 * \mathcal{R}_2^1$$

where, \mathcal{H}_2^1 is the homogeneous transformation matrix of axes 2 with respect to axis 1, which is obtained by translation \mathcal{T}_2^1 followed by rotation \mathcal{R}_2^1 . The rest of the notations are similar.

$$\mathcal{H}_2^1 = \begin{bmatrix} 1 & 0 & 0 & -(x_4 - x_3) \\ 0 & 1 & 0 & y_1 \\ 0 & 0 & 1 & h \\ 0 & 0 & 0 & 1 \end{bmatrix} \begin{bmatrix} 1 & 0 & 0 & 0 \\ 0 & \cos\theta & -\sin\theta & 0 \\ 0 & \sin\theta & \cos\theta & 0 \\ 0 & 0 & 0 & 1 \end{bmatrix}$$

$$\mathcal{H}_3^2 = \mathcal{T}_3^2 * \mathcal{R}_3^2$$

$$\mathcal{H}_3^2 = \begin{bmatrix} 1 & 0 & 0 & 0 \\ 0 & 1 & 0 & y_2 \\ 0 & 0 & 1 & 0 \\ 0 & 0 & 0 & 1 \end{bmatrix} \begin{bmatrix} \cos\frac{\phi}{2} & \sin\frac{\phi}{2} & 0 & 0 \\ -\sin\frac{\phi}{2} & \cos\frac{\phi}{2} & 0 & 0 \\ 0 & 0 & 1 & 0 \\ 0 & 0 & 0 & 1 \end{bmatrix}$$

$$\mathcal{H}_4^3 = \mathcal{T}_4^3 * \mathcal{R}_4^3$$

$$\mathcal{H}_4^3 = \begin{bmatrix} 1 & 0 & 0 & (x_4 - x_3) \\ 0 & 1 & 0 & (y_3 - y_4) \\ 0 & 0 & 1 & -h \\ 0 & 0 & 0 & 1 \end{bmatrix} \begin{bmatrix} 1 & 0 & 0 & 0 \\ 0 & 1 & 0 & 0 \\ 0 & 0 & 1 & 0 \\ 0 & 0 & 0 & 1 \end{bmatrix}$$

$$\mathcal{H}_4^1 = \mathcal{H}_2^1 * \mathcal{H}_3^2 * \mathcal{H}_4^3 \quad (3.1)$$

Thus, from equation 3.1, we obtain the homogeneous transformation matrix of coordinate axis-4 with respect to the coordinate axis-1, i.e. \mathcal{H}_4^1 .

$$\mathcal{H}_4^1 = \begin{bmatrix} C(\frac{\phi}{2}) & S(\frac{\phi}{2}) & 0 & \bar{y}_{34}S(\frac{\phi}{2}) - \bar{x}_{43}(1 - C(\frac{\phi}{2})) \\ -S(\frac{\phi}{2})C(\theta) & C(\frac{\phi}{2})C(\theta) & -S(\theta) & y_1 + hS(\theta) + y_2C(\theta) + \bar{y}_{34}C(\frac{\phi}{2})C(\theta) - \bar{x}_{43}S(\frac{\phi}{2})C(\theta) \\ -S(\frac{\phi}{2})S(\theta) & C(\frac{\phi}{2})S(\theta) & C(\theta) & h(1 - C(\theta)) + y_2S(\theta) + \bar{y}_{34}C(\frac{\phi}{2})S(\theta) - \bar{x}_{43}S(\frac{\phi}{2})S(\theta) \\ 0 & 0 & 0 & 1 \end{bmatrix}, \quad (3.2)$$

where $C(\cdot) = \cos(\cdot)$; $S(\cdot) = \sin(\cdot)$; $\bar{x}_{43} = x_4 - x_3$; $\bar{y}_{34} = y_3 - y_4$

We know that the homogeneous coordinate of A w.r.t. O_4 is given by:

$$O_4A = \begin{bmatrix} 0 \\ 0 \\ 0 \\ 1 \end{bmatrix},$$

Thus, using the homogeneous matrix \mathcal{H}_4^1 , we can obtain the coordinates of point A w.r.t O_1 .

$$O_1A = \mathcal{H}_4^1 * O_4A$$

$$O_1A = \begin{bmatrix} \bar{y}_{34}S(\frac{\phi}{2}) - \bar{x}_{43}(1 - C(\frac{\phi}{2})) \\ y_1 + hS(\theta) + y_2C(\theta) + \bar{y}_{34}C(\frac{\phi}{2})C(\theta) - \bar{x}_{43}S(\frac{\phi}{2})C(\theta) \\ h(1 - C(\theta)) + y_2S(\theta) + \bar{y}_{34}C(\frac{\phi}{2})S(\theta) - \bar{x}_{43}S(\frac{\phi}{2})S(\theta) \\ 1 \end{bmatrix}, \quad (3.3)$$

We assume, (1) the tendons are inextensible, and (2) they remain taut, even in the unactuated position,i.e. when θ is 0° . Thus, ideally, its length \mathcal{L} will remain unchanged for all the states and will be equal to,

$$\mathcal{L} = y_1 + y_2 + \bar{y}_{34} \quad (3.4)$$

The distance between O_1 and A is given by,

$$\overline{O_1A} = \sqrt{(O_1A)_x^2 + (O_1A)_y^2 + (O_1A)_z^2} \quad (3.5)$$

where,

$$\begin{aligned} (O_1A)_x &= \bar{y}_{34}\mathcal{S}\left(\frac{\phi}{2}\right) - \bar{x}_{43}(1 - C\left(\frac{\phi}{2}\right)) \\ (O_1A)_y &= y_1 + h\mathcal{S}(\theta) + y_2C(\theta) + \bar{y}_{34}C\left(\frac{\phi}{2}\right)C(\theta) - \bar{x}_{43}\mathcal{S}\left(\frac{\phi}{2}\right)C(\theta) \\ (O_1A)_z &= h(1 - C(\theta)) + y_2\mathcal{S}(\theta) + \bar{y}_{34}C\left(\frac{\phi}{2}\right)\mathcal{S}(\theta) - \bar{x}_{43}\mathcal{S}\left(\frac{\phi}{2}\right)\mathcal{S}(\theta). \end{aligned}$$

Thus,

$$\boxed{\overline{O_1A} = \mathcal{L}} \quad (3.6)$$

Substituting from the equations 3.4 and 3.5 in the equation 3.6, we get a relationship between θ and ϕ . Clearly, the output angle ϕ is an implicit function of the input angle θ . That is,

$$\boxed{\phi = f(\theta, \phi \mid y_1, y_2, y_3, y_4, x_3, x_4, h)} \quad (3.7)$$

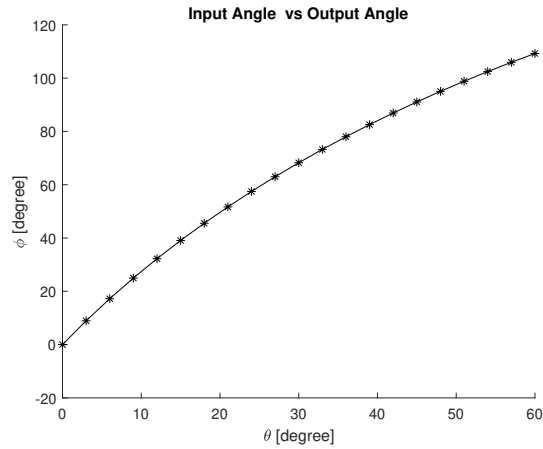


Figure 3.5: The plot showing the relationship between the input angle and the output angle.

Note: This plot is obtained by taking the values of our microgripper design parameters which are mentioned in the next section.

3.3 Workspace of the microgripper

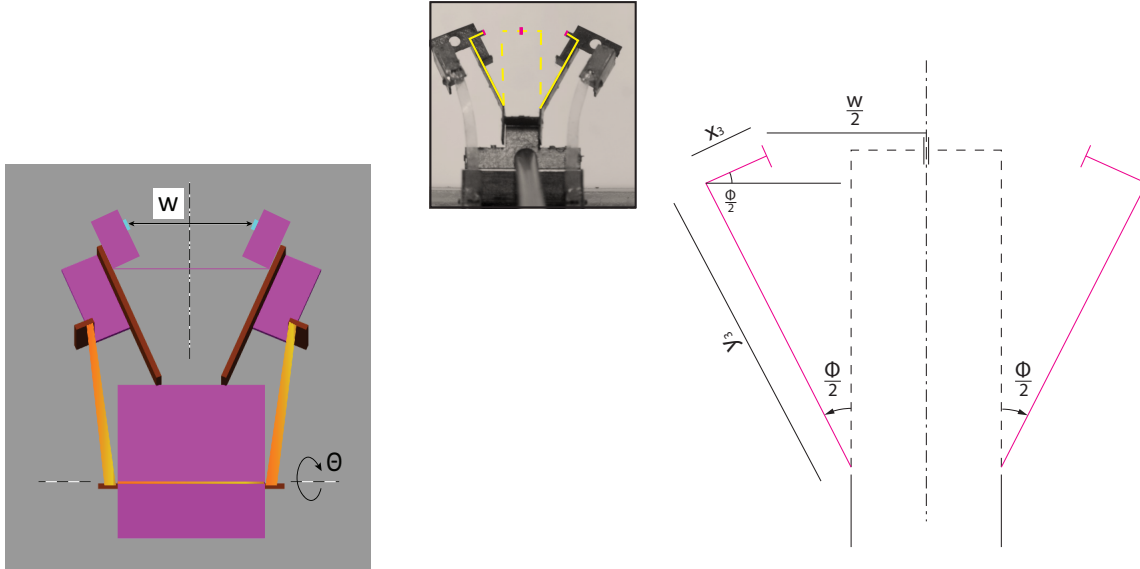


Figure 3.6: The top view of the gripper, showing the jaw opening.

The trajectory of the gripper jaw tip with respect to the base link-1 at axis-2 gives the workspace of the gripper, $(x_{jaw}, y_{jaw}, z_{jaw})$. They are given by,

$$x_{jaw, left} = (y_3 \sin \frac{\phi}{2} + x_3(1 - \cos \frac{\phi}{2})) ; \text{ for the left jaw tip.} \quad (3.8)$$

$$x_{jaw, right} = -(y_3 \sin \frac{\phi}{2} + x_3(1 - \cos \frac{\phi}{2})) ; \text{ for the right jaw tip.} \quad (3.9)$$

$$y_{jaw} = (y_2 + y_3) \cos \theta \quad (3.10)$$

$$z_{jaw} = (y_2 + y_3) \sin \theta \quad (3.11)$$

Thus, we obtain the gripper jaw opening, w given by,

$$w = x_{jaw, left} - x_{jaw, right}$$

$$w = 2 \left(y_3 \sin \frac{\phi}{2} + x_3 \left(1 - \cos \frac{\phi}{2} \right) \right) \quad (3.12)$$

Obtaining the pair (w, z_{jaw}) is crucial for finding the range of size of objects the gripper, with specific design parameters, is capable of grasping. This does not guarantee the success of grasping the target object; rather, this indicates whether there can be any contact established between the gripper's jaw tips and the target object or not.

The dimensions of the various design parameters of our micro-gripper are as follows:

Our chosen microgripper design parameters

$$y_1 = 0.075 \text{ mm}$$

$$y_2 = 5.25 \text{ mm}$$

$$y_3 = 7.675 \text{ mm}$$

$$y_4 = 4.2427 \text{ mm}$$

$$x_3 = 1.65 \text{ mm}$$

$$x_4 = 3.75 \text{ mm}$$

$$h = 3.25 \text{ mm}$$

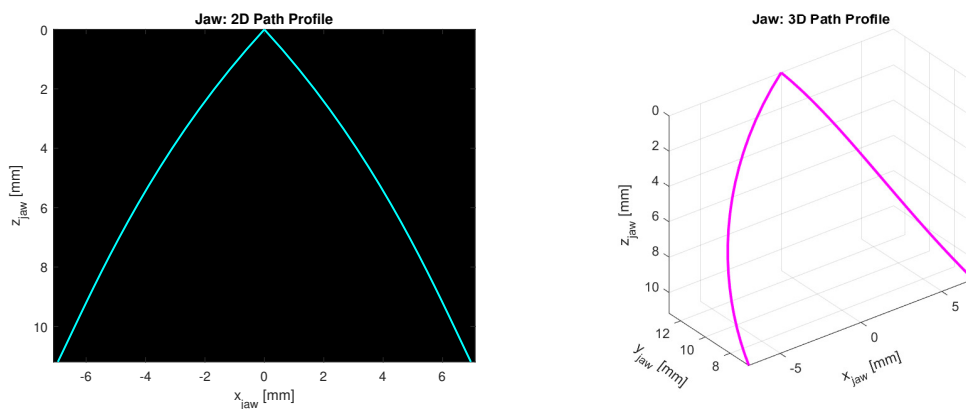


Figure 3.7: Jaw Path Profile w.r.t axis-2.

In figure 3.7, we demonstrate the trajectory of our microgripper's jaw tip with respect to the base link at coordinate axis-2. Clearly, we notice that the gripper would fail to grasp any

object that lies within its jaw profile path. It is the first step to ensure that the cross-section of the target object which is at some level from gripper base link exceeds the bound between the tip trajectories at that same level. It is then when any chance of grasping would be possible.

3.4 Experiments and Results

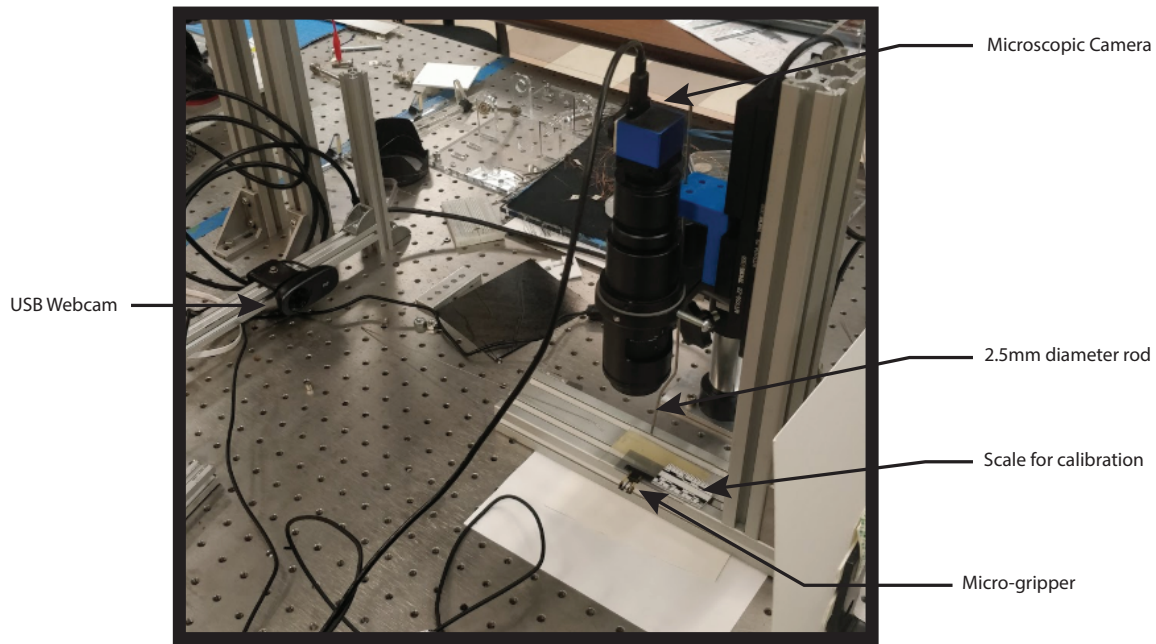


Figure 3.8: Experimental Setup.

In order to validate the input-output angle relationship (equation 3.7) that we have already established, we performed an experiment with our microgripper. The experimental setup consisted of two cameras, one located above the gripper and the other at the side as shown in the figure 3.8. The camera on the top was calibrated to measure the jaw opening of the gripper. The camera at the side was used to measure the input hinge angles of the gripper. Figure 3.9 shows a few samples of the input angle-jaw opening pairs. The gripper was mechanically actuated using a 2.5 mm diameter rod. The experiment was run 82 times over 1 complete cycle.

Next we plotted the experimental values of the jaw opening for various input hinge

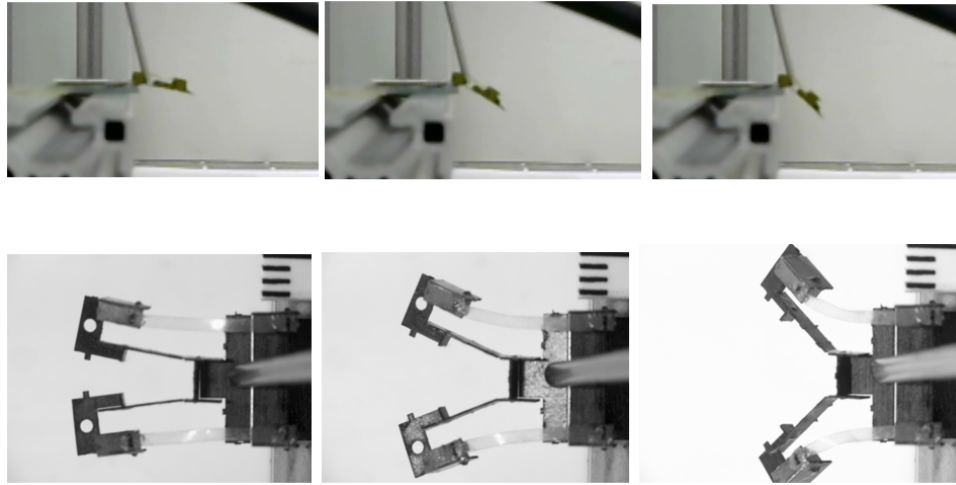


Figure 3.9: Samples from the experiment. The top row shows the input angles. The bottom row displays the gripper jaw opening.

angles and compared it with the analytical model (equations 3.7 and 3.12) using MATLAB. The plot shown in figure 3.10 shows that the theoretical result matches pretty well with the experimental result. The small deviations could arise due to the assumptions taken in modeling the gripper, experimental errors, manufacturing defects. The assumptions taken while deriving the mathematical model are (1) the links are perfectly rigid, (2) the tendons are inextensible, (3) the hinges behave like a revolute joints without any stretching. The experimental uncertainties arises due to (1) extracting information such as input angles and jaw openings from images, and (2) calibrating the microscopic camera that is located above the gripper only once. That is when the gripper is not actuated. As a result of bending of the gripper about the input hinge joint, the distance between the gripper tips and the camera changes. It is assumed that the displacements of the jaw tips from the camera are not very large and that is true for small gripper size. Some of the manufacturing defects or limitations involve (1) the tendons having a finite width and getting twisted when the gripper is actuated, (2) the tendons having some slack in the initial unactuated state, i.e. , when θ is 0° .

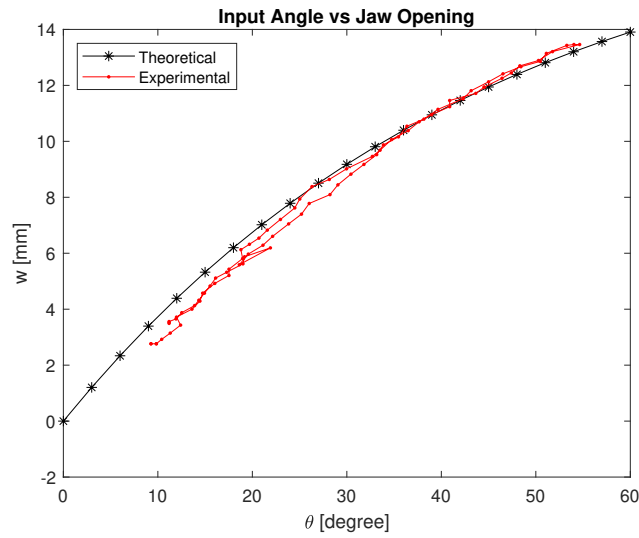


Figure 3.10: Experimental Validation.

In order to further confirm the validity of our analytical model of the gripper, we ran a simulation in MathWorks Simscape. The Simscape multibody model of our microgripper in the Simulink is shown in figure 3.11. The plot in the figure 3.12 presents the analytical model and

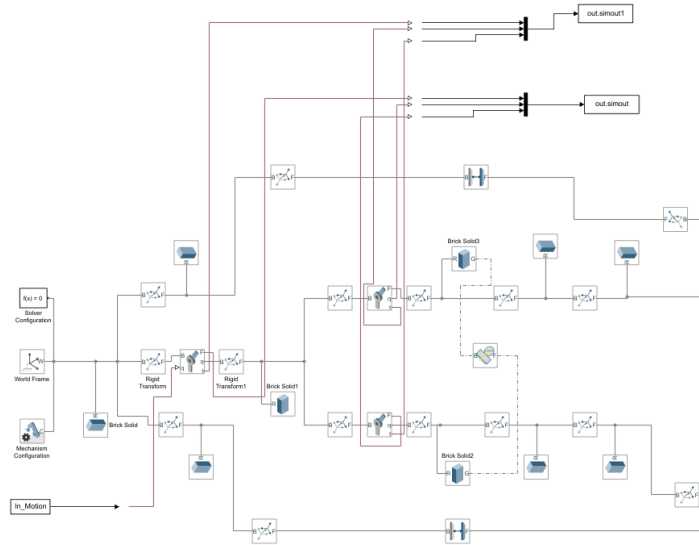


Figure 3.11: Simulation in MathWorks Simscape.

shows that it is in excellent agreement with simulation data generated from the Simscape model. This confirms that our analytical model is correct.

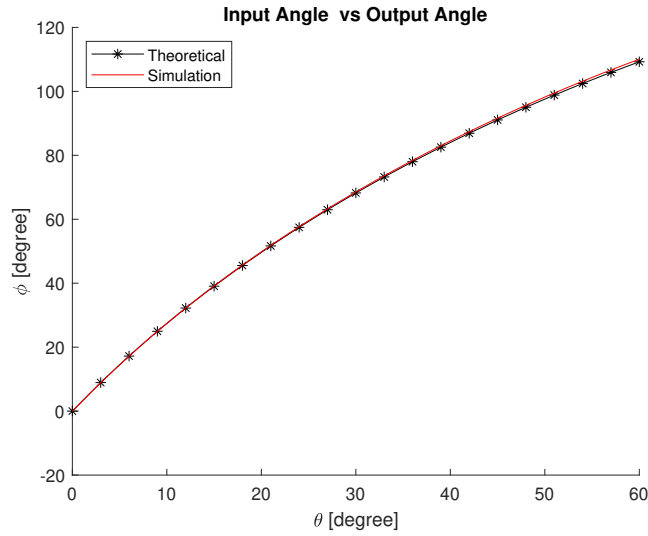


Figure 3.12: Simulation Validation.

3.5 Kinematic Ratio of the microgripper

The Kinematic Ratio of the gripper helps us to understand by how much the actuator needs to displace in order to obtain a desired displacement at the gripper jaw tips. This would also give an insight for the actuator selection for the gripper and also can be useful in position control of the gripper jaw tip.

$$KR_{gripper} = \frac{\frac{d\phi}{dt}}{\frac{d\theta}{dt}}$$

On simplifying,

$$\boxed{KR_{gripper} = \frac{d\phi}{d\theta}} \quad (3.13)$$

. The plot of $KR_{gripper}$ versus θ clearly shows that kinematic ratio keeps decreasing with the increase in the input hinge angle. However, $KR_{gripper}$ is always greater than 1, which shows the amplification of the output angle for a given input angle. It is desirable for small-sized actuators or actuators with poor or moderate strains.

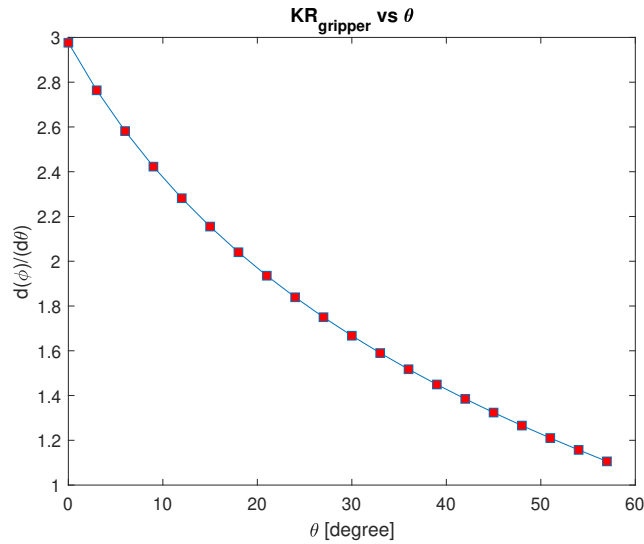


Figure 3.13: Kinematic Ratio of the gripper

3.6 Influence due to the various Design Parameter

By now we have realised the importance of the design parameters in the modeling of the gripper. It is therefore crucial to understand the influence of the various design parameters on the workspace of the gripper. This would also help us in developing different object-specific grippers.

Increase of	y_1	y_2	y_3	y_4	x_3	x_4	h
ϕ	decreases	decreases	decreases	increases	increases	decreases	increases
w	decreases	decreases	increases	increases	increases	decreases	increases

Table 3.1: Summary of the influence of the various design parameters on the output angle and jaw opening.

- y_1 : As y_1 decreases, ϕ increases, and thus the jaw opening, w increases. In our design we have thus chosen y_1 to be as small as possible.
- y_2 : As y_2 decreases, ϕ increases, and thereby the jaw opening increases. We notice that influence of y_2 on jaw opening is the least among all the design parameters. It's dimension is chosen based on the actuator's area of contact with the gripper. Initial plan was to use a similar piezoelectric actuator that is used in the P3 robot. The dimension of the PZT

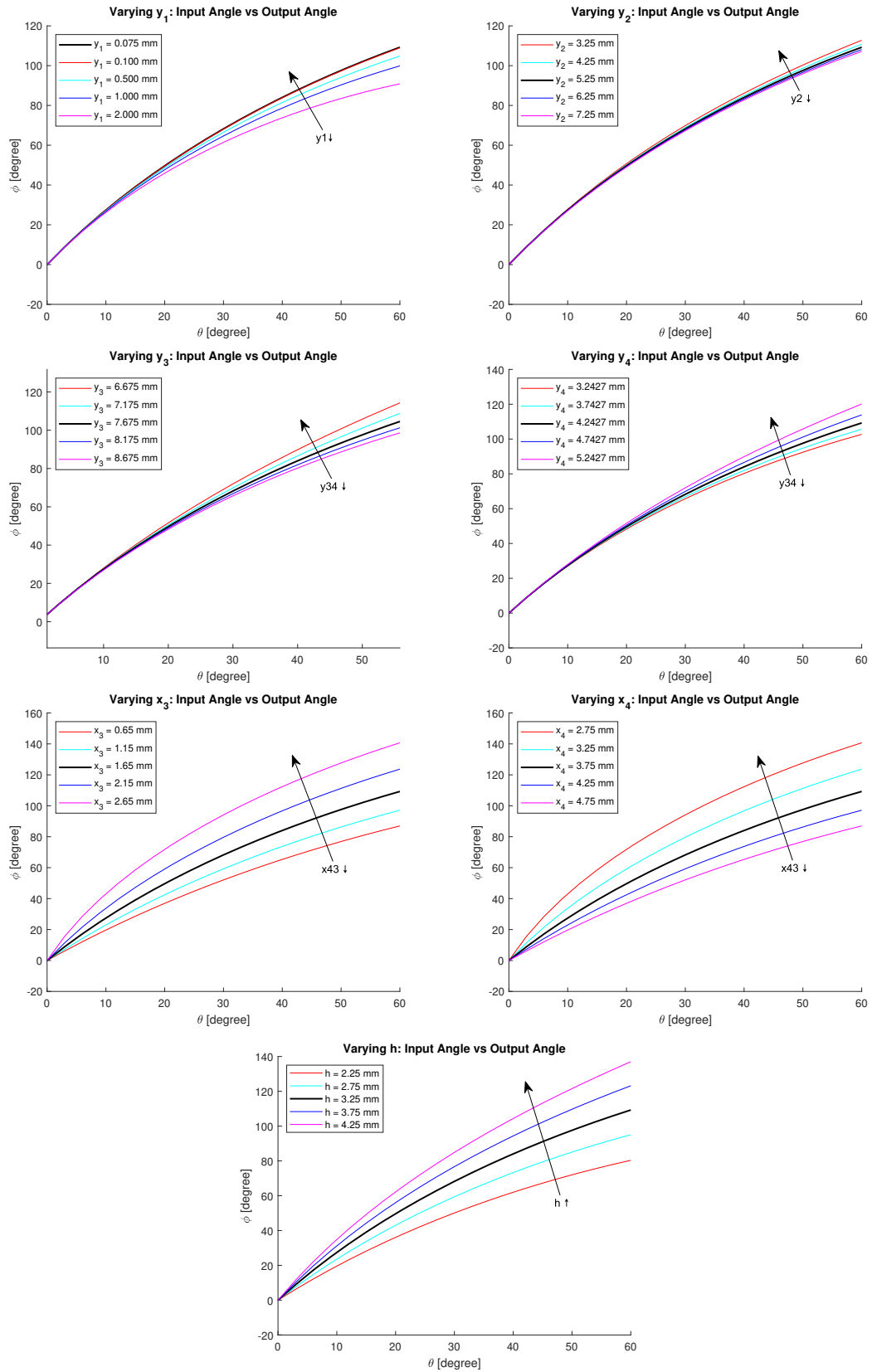


Figure 3.14: Influence of the Design Parameters on Output Angle.

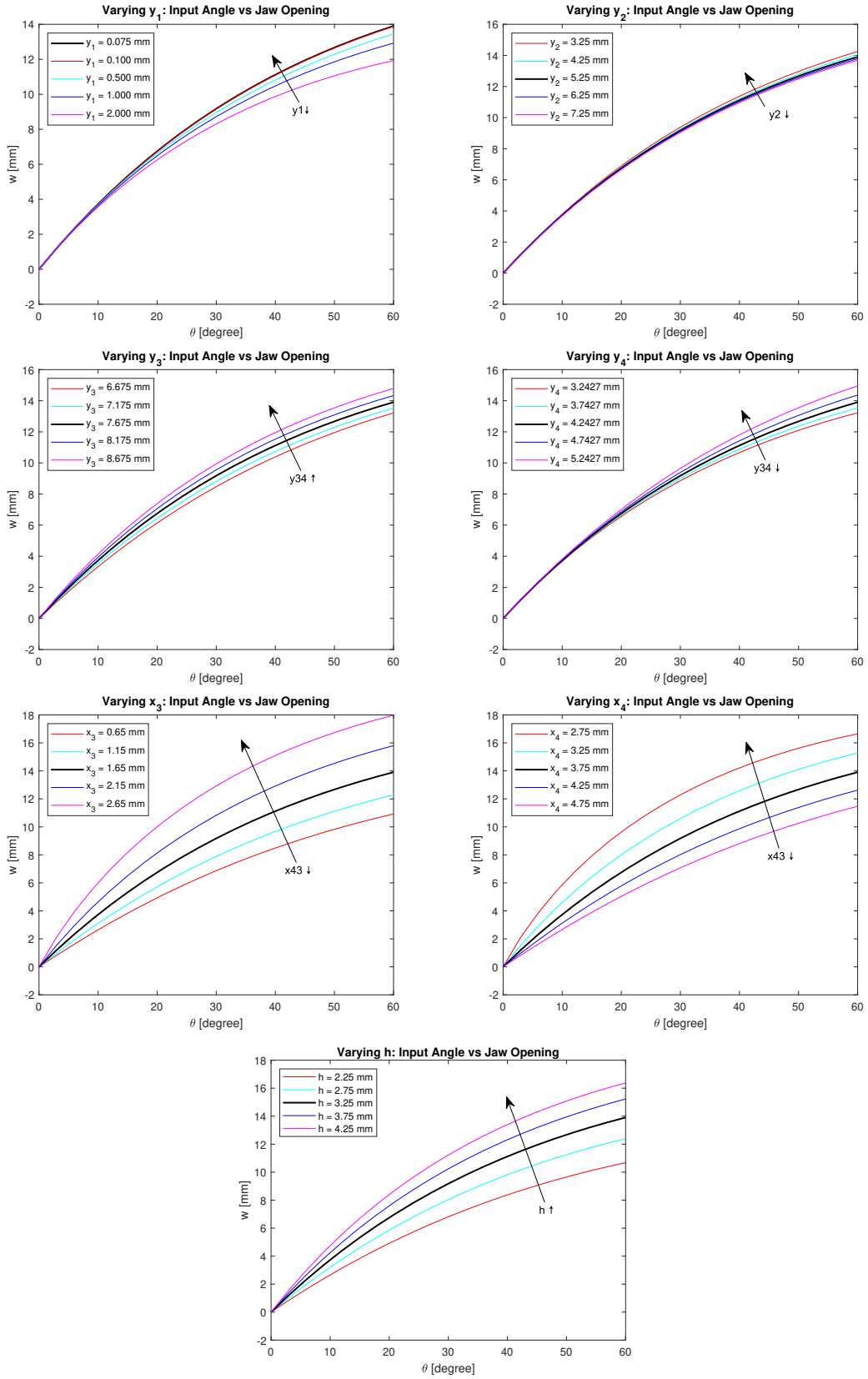


Figure 3.15: Influence of the Design Parameters on Jaw Opening.

actuator tip is $1.5\text{mm} \times 3\text{mm}$. Also, there is a length of offset equal to 1.28 mm from the output hinges to the link-2, on which the actuator can make an area of contact. Thus, $y_2 > 3 + 1.28\text{ mm}$ was chosen.

- **y₃** : As y_3 increases, jaw opening may increase, even though ϕ decreases. This can also be understood by carefully observing the jaw opening equation 3.12. Increasing y_3 would also result in the increase of the size of the gripper.
- **y₄**: With the increase in y_4 , ϕ increases and thus jaw opening increases. This would result in the shorter tendon size and result in more stress at the output hinge joints. It must be noted that there is a limit of rotation that a conventional flexure can go through before yielding [WAS⁺08].
- **x₃**: As x_3 increases, the value of ϕ and w increases significantly. There are design limitations for increasing x_3 . That is, there needs to be supporting materials on both the sides of the output hinges until the release cut in the design process.
- **x₄**: As x_4 decreases, the value of ϕ and w increases significantly. This suggests that upon decreasing the distance between the tendons, the jaw opening would be greater. But it comes at a price of higher stresses at the output hinge joints.
- **h**: As expected, the value of ϕ and w increases with increase in h . This design parameter can be utilised to amplify the *kinematic ratio* of the gripper, keeping the area occupied by the gripper unchanged.

3.7 Configuration Space of the microgripper: A case study

Some of the chosen target objects for the microgripper to grasp were the standard hexagonal nuts, which are shown in the figure 3.16. It is difficult for the gripper to grasp the hex nuts when they are lying down (as shown in the left image of figure 3.16) as compared to when they are in standing position, i.e. , on their flats (as shown in the right image of 3.16). There are two reasons for that. First, it is likely to fall within the gripper jaw tip profile, in which case there would not be any contact established. This is because the gripper attached on top of the P3 robot, whose height is about 7.5 mm , has to bend a significant amount, resulting in a wide jaw opening. The second major reason is that there will be a large force (discussed in the next chapter), $2 \times F_{\text{pushing_away}}$, responsible for pushing the nut away from the gripper .

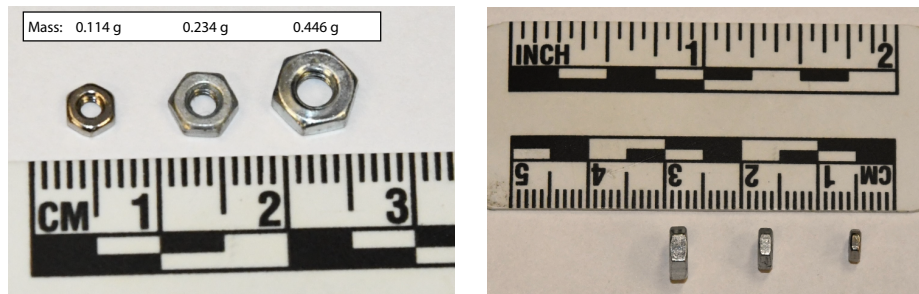


Figure 3.16: Specifications of some of the target objects for grasping.

Here, we would be demonstrating the configuration space or joint space (θ, ϕ) of our microgripper when the target object is the largest one among the three hexagonal nuts, in its standing position. It is a M3.5 hexagonal nut that weighs m_{nut} , 0.446 grams. The thickness of the nut t_{nut} , is 2.8 mm and it's width across flats s_{nut} , is 6.0 mm.

During grasping the jaw opening of the gripper must be equal to the thickness of the nut in order to establish contact, i.e. ,

$$w = t_{nut}$$

. Using equation 3.12, we solve for ϕ .

$$2 \left(y_3 \sin \frac{\phi}{2} + x_3 \left(1 - \cos \frac{\phi}{2} \right) \right) = 2.8$$

Thus, we get $\phi = 20.6161^\circ$. Then with the help of MATLAB, we calculate the value of θ by solving the relationship derived between θ and ϕ :

$$\theta = g(\phi, \theta \mid y_1, y_2, y_3, y_4, x_3, x_4, h)$$

θ comes out to be equal to 7.2911° . Next plugging the value of θ in the equation of z_{jaw} [3.11], we find its value to be 1.6403 mm. This along with the s_{nut} value is important in deciding the level of the base link of the gripper in order to make contact with the nut. If the nut is at the ground level then,

$$1.6403 \text{ mm} < \text{link-1 level from ground} < 1.6403 \text{ mm} + 6.00 \text{ mm}$$

$$1.6403 \text{ mm} < \text{link-1 level from ground} < 7.6403 \text{ mm}$$

We know that the height of the P3 robot is 7.5 mm, which makes the gripper suitable for grasping the nut when lying on its flat.

If we calculate the same for the hexagonal nut, when it is lying down, we need to have $w = s_{nut}$, and thus we get $\phi = 44.0703^\circ$, $\theta = 17.3016^\circ$ and $z_{jaw} = 3.8439$ mm. Now if the nut is at the ground level the thickness of the nut, t_{nut} plays an important role in determining if the contact is been established or not. In order to make contact

$$3.8439 \text{ mm} < \text{link-1 level from ground} < 3.8439 \text{ mm} + 2.8 \text{ mm}$$

$$3.8439 \text{ mm} < \text{link-1 level from ground} < 6.6439 \text{ mm}$$

As the base link of the gripper needs to be at height lower than the height of P3 robot, i.e. 7.5 mm, the gripper fails to grasp the nut in this orientation.

Also, we would like to point out that for the other two smaller hexagonal test nuts, they need to be some distance above the ground level of the P3 robot in order establish contact with the gripper.

The static analysis of the microgripper on the hexagonal nut is done in the next chapter in section 4.6, where the rest of the determining factors are studied in order to infer on the success of picking up the hex nut.

Chapter 4

Static Analysis

4.1 Background

In the previous chapter, we have discussed about the necessary design parameters that are crucial for determining whether contact between the target object and the gripper tips can be established or not. In addition to this, we also need to perform the static analysis of the gripper in order to understand the other design parameters that are important to ensure its success of grasping. The reason for this is even after contact has been made, the object may still slip. Thus we need to find the force crucial for grasping the object, F_{output} . We also need to find the actuator force as it would be helpful in actuator selection.

4.2 Flexure Stiffness of the hinge joints

First we need to determine the stiffness of all the hinge joints in the gripper. As mentioned in the paper [DGS⁺15], the bending stiffness of uncastellated flexure is given by,

$$k = \frac{E_k b t^3}{12l} \quad (4.1)$$

E_k is the Young's modulus of Kapton (2.5 GPa), b is the width of flexure, t is the thickness and l is the length. As shown in figure 2.1, the gripper design consists of three revolute joints, which are actually hinges made of flexural Kapton layer.

Thus using equation 4.1, the hinge stiffness of the input joint (k_{in}), i.e. the joint linking link-1 and link-2, is:

$$k_{in} = \frac{(2.5 \text{ GPa}) \times 10^9 \times (7.5 \text{ mm}) \times 10^{-3} \times ((0.0762 \text{ mm}) \times 10^{-3})^3}{12 \times (0.15 \text{ mm}) \times 10^{-3}} = 4.6 \times 10^{-3} \text{ N.m}$$

as $b = x_1 = 7.5 \text{ mm}$, $t = 0.0762 \text{ mm}$ for DUPONT* 300HN Kapton polyimide film, and $l = 0.15 \text{ mm}$, which is a gap length chosen for our hinge design.

Similarly, the hinge stiffness of each of the output revolute joints (k_{out}), i.e. the joint linking link-2 and link-3, is:

$$k_{out} = \frac{(2.5 \text{ GPa}) \times 10^9 \times (1.45 \text{ mm}) \times 10^{-3} \times ((0.0762 \text{ mm}) \times 10^{-3})^3}{12 \times (0.15 \text{ mm}) \times 10^{-3}} = 0.89105 \times 10^{-3} \text{ N.m}$$

, where $b = z_1$ (see figure 2.1) = 1.45 mm.

4.3 Actuation Force

This is crucial for selecting the actuator that for the gripper. It is desirable to have a low actuation force in order to actuate the gripper, as higher force would generally mean a large size of the actuator. It would also mean more energy required to actuate the gripper. Ideally, we would aim for an actuator with high work density for the microgripper.

Actuation Force Calculation: Assuming a constant force is applied to actuate the gripper and its direction is always normal to the surface of link-2, we can compute the average actuator force $\langle F_{actuator} \rangle$ that will be required using the energy balance theorem.

*<https://www.dupont.com/products/kapton-hn.html>

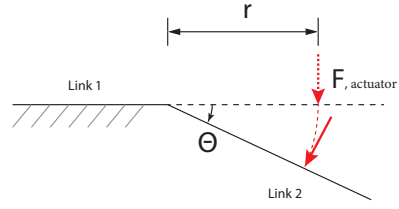
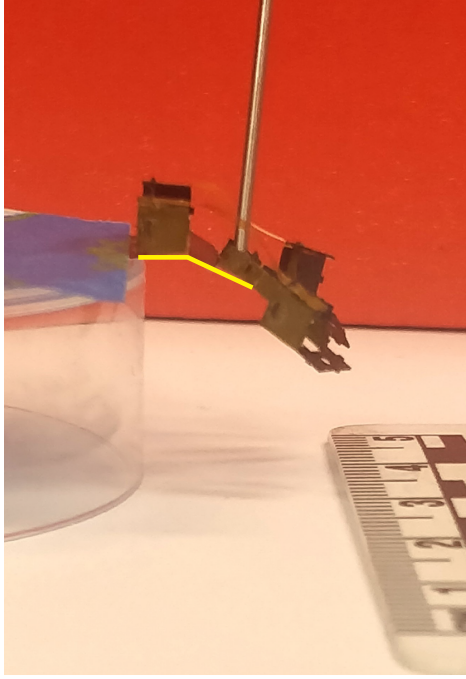


Figure 4.1: Input force required to actuate the gripper.

Assuming no dissipative energy losses, the work done by the actuator will be stored as elastic potential energy in the hinge joints. Thus we can write,

$$\langle F_{actuator} \rangle (r\theta) = \frac{1}{2}k_{in}(\theta)^2 + 2 \left(\frac{1}{2}k_{out} \left(\frac{\phi}{2} \right)^2 \right)$$

where, $F_{actuator}$ is in *Newton*, when θ and ϕ are in *radians*, and r in *meters*. r is the distance from the base link-1 to the actuator's point of force application on link-2, as shown in the figure 4.1.

Thus,

$$0 < r < y_2$$

Due to design constraints, r is actually some length lower than y_2 , i.e. $r = y_2 - \text{offset}$. In our design the length of this offset is 1.28 mm. Thus, $r_{max} = 5.25 - 1.28 = 3.97 \text{ mm}$. The offset distance depends on the output hinge location and also on the output hinge width, z_3 . Clearly, it is preferable to set r as large as possible, so that $F_{actuator}$ required to drive the gripper is the least.

Another thing to notice here is that the actuation force calculated above is not the instantaneous one, rather it is the average actuation force. This is because initially when the hinges were in relaxed position, the force applied would be zero and it would gradually increase with the bending of the hinges.

In order to obtain the instantaneous value of $F_{actuator}$, we used Castigliano's first theorem which states that, "The first partial derivative of the total internal energy (strain energy) in a structure with respect to any particular deflection component at a point is equal to the force applied at that point and in the direction corresponding to that deflection component."[†]

$$F_{actuator} = \frac{\partial(\frac{1}{2}k_{in}(\theta)^2 + 2 \times (\frac{1}{2}k_{out}(\frac{\phi}{2})^2))}{\partial(r\theta)}$$

On simplifying the equation, we get

$$F_{actuator} = \frac{1}{r}(k_{in}\theta + k_{out}\frac{\phi}{2}\frac{\partial\phi}{\partial\theta}) \quad (4.2)$$

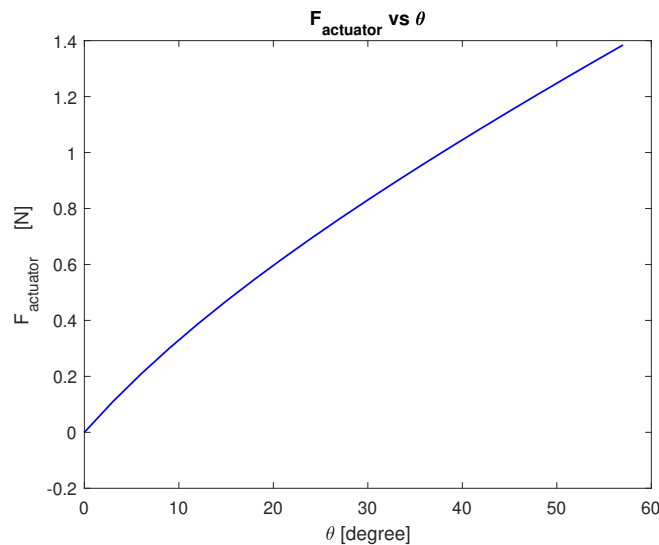


Figure 4.2: Actuation force plot

[†]https://engineering.purdue.edu/~ce474/Docs/The%20Theorem%20of%20Least%20Work_2012.pdf

We see that around 1.4 N force is required to actuate the micro-gripper all the way to $\theta = \pi/3$.

4.4 Grasping Force

Analyzing the force with which the gripper grasps a target object is of utmost importance. It could either damage a delicate object or fail to pick a heavy object if not chosen properly. Hence we focus on finding the output force generated by the gripper at its jaw tip.

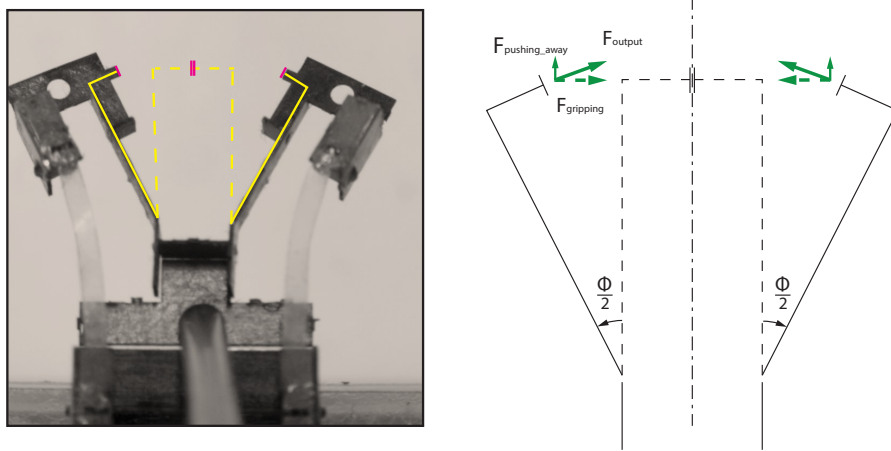


Figure 4.3: Gripping Contact Force of the gripper.

As shown in figure 4.3, the output gripper force F_{output} , can be resolved into two components. The $F_{gripping}$ component is crucial in determining whether it would be safe to handle a delicate object or whether it is strong enough to pick an object of certain weight and texture. The undesired $F_{pushing_away}$ component is responsible for pushing the target object away from the gripper, and it increases with wider jaw openings.

$$\vec{F}_{output} = \vec{F}_{gripping} + \vec{F}_{pushing_away} \quad (4.3)$$

, where

$$F_{\text{gripping}} = F_{\text{output}} \cos \frac{\phi}{2}$$

$$F_{\text{pushing_away}} = F_{\text{output}} \sin \frac{\phi}{2}$$

Due to opening of the jaws, there is a restoring torque, τ , at the output jaw openings that is given by:

$$\tau = k_{\text{out}} \frac{\phi}{2} \quad (4.4)$$

Balancing the net moment about the output hinge,

$$F_{\text{output}} y_3 = \tau$$

$$F_{\text{output}} = \frac{\tau}{y_3}$$

Hence, we get

$$F_{\text{output}} = \frac{1}{y_3} k_{\text{out}} \frac{\phi}{2} \quad (4.5)$$

, where F_{output} is in N , when y_3 is in m and ϕ is in *radian*.

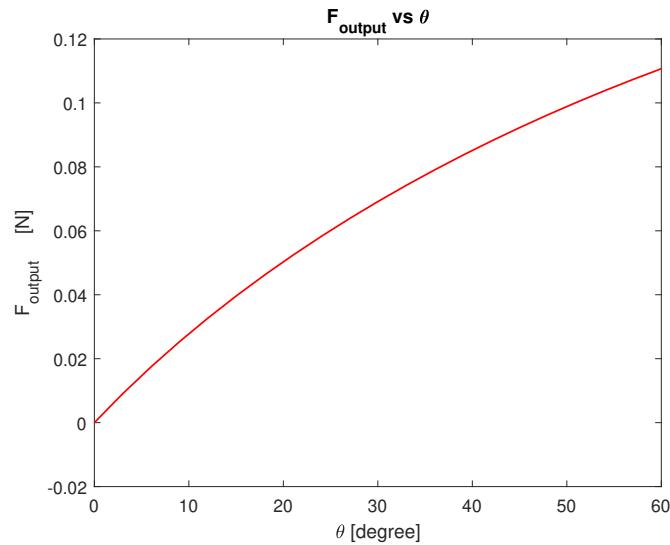


Figure 4.4: Output force plot

As expected the output force increases with the bending of the input hinge joint, due to the larger restoring torque generated at the output hinges. However, the magnitude of output force is quite small compared to the actuation force.

4.5 Mechanical Advantage of the microgripper

In order to get a better picture of the magnitude of the output force in comparison to the magnitude of the force required to actuate of the gripper, the force plots are combined into one and shown in figure 4.5.

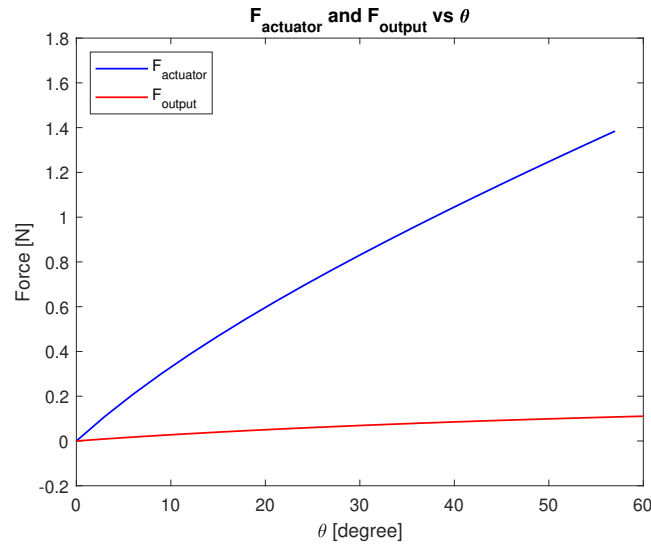


Figure 4.5: Actuator force and Output force.

A better way to compare the output force with respect to the input force of a mechanical system is through its Mechanical Advantage. The Mechanical Advantage of the gripper, i.e. $MA_{gripper}$, is given by:

$$MA_{gripper} = \frac{F_{output}}{F_{actuator}} \quad (4.6)$$

With the help of equations 4.2 and 4.5 we get,

$$MA_{gripper} = \frac{\frac{1}{y_3} k_{out} \frac{\phi}{2}}{\frac{1}{r} (k_{in} \theta + k_{out} \frac{\phi}{2} \frac{\partial \phi}{\partial \theta})}$$

Using equation 3.13, we can write

$$MA_{gripper} = \frac{\frac{1}{y_3} k_{out} \frac{\phi}{2}}{\frac{1}{r} (k_{in} \theta + k_{out} \frac{\phi}{2} \cdot KR_{gripper})} \quad (4.7)$$

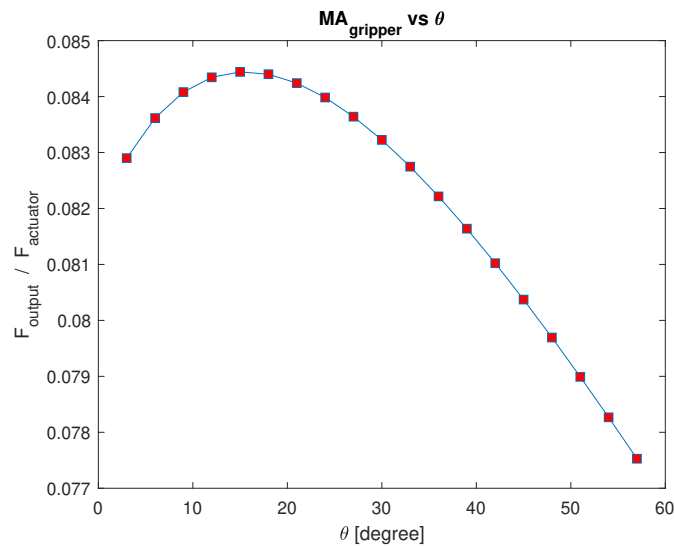


Figure 4.6: Mechanical Advantage of the gripper

Figure 4.6 clearly shows that Mechanical Advantage of the microgripper is always less than 1. Depending on the type of object the gripper is handling, for instance, how delicate the object is, the force might be enough or there might be a demand for a greater output force.

4.6 Static Analysis on the hexagonal nut

In the previous chapter in section 3.7, it is proven that the contact between the gripper jaw tip and the target hexagonal nut can be made when it is standing on its flat. Once the contact is

established the tension of the tendons becomes zero. The restoring torque, τ , at the output hinge joints are (see equation 4.4):

$$\tau = 0.89105 \times 10^{-3} \text{ N.m} \times \frac{20.6161^\circ}{2} \times \frac{\pi \text{ radians}}{180^\circ} = 1.6031 \times 10^{-4} \text{ N.m}$$

Next using equation 4.5,

$$F_{\text{output}} = \frac{1.6031 \times 10^{-4} \text{ N.m}}{7.6750 \text{ mm} \times 10^{-3}}$$

$$F_{\text{output}} = 0.0209 \text{ N}$$

Also, we notice that the component of the force, $F_{\text{pushing_away}}$, is small. To be precise 0.0037 N. Thus a net force of 0.0074 N will be acting to push the nut away from the gripper along a plane that is parallel to the plane containing the link-2 of the microgripper.

In order to pick the hexagonal nut, the gripper must be able to lift the weight of the nut. It is clear that the coefficient of friction between the end-effector of the gripper and the hex nut, μ , plays a vital role.

$$2\mu F_{\text{output}} = m_{\text{nut}} g$$

$$2\mu \times 0.0209 \text{ N} = 0.446 \text{ gm} \times 10^{-3} \times 9.8 \text{ m/s}^2$$

On solving we get,

$$\mu = 0.1047$$

Thus the minimum coefficient of limiting friction required at the contact is 0.1047. The gripper tip (shown in 4.12.(f)) is modular and was made out of carbon fiber. The coefficient of friction for Carbon-Steel combination[‡] in clean and dry surface conditions is 0.14 and that in lubricated and greasy is 0.11 - 0.14. Thus the gripper barely manages to pick the hexagonal nut.

As our target object, which is a hexagonal nut, is not delicate, we can afford to have higher

[‡]https://www.engineeringtoolbox.com/friction-coefficients-d_778.html

output forces for a stronger grip.

4.6.1 Gripper Modifications

We see that there is a need to modify the gripper so that it is able to have a more firm grasp on the hexagonal test nut. As the contact between the gripper tips and the nut have been established, we need to modify the gripper without changing the kinematics of it. There are a few ways to do.

1. The flexure designs output hinges can be castellated [DGS⁺15], in order to increase the stiffness of those hinges. This would mean a slight increase of the actuation force as well.

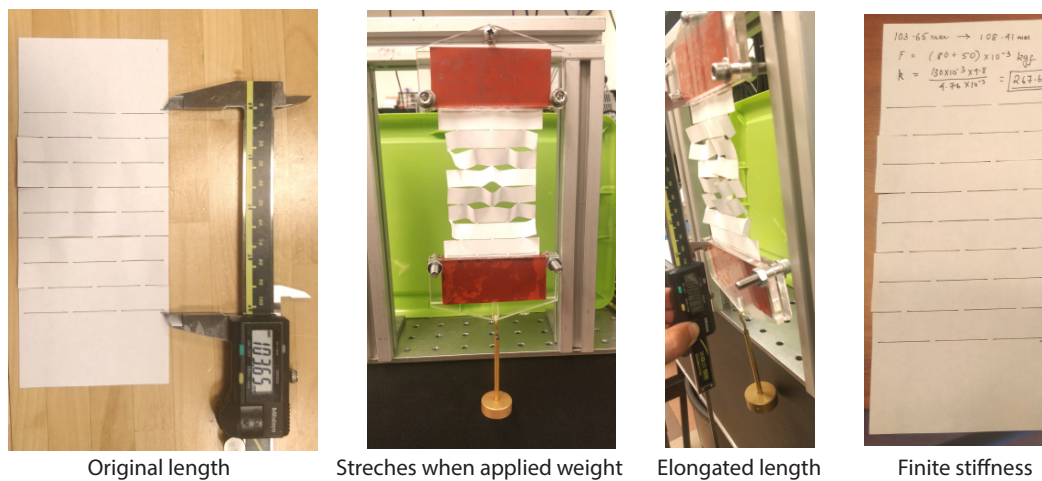


Figure 4.7: A simple experiment demonstrating the elasticity in a kirigami structure.

2. Inspired by the art of paper cutting, kirigami provides tools to create materials with unconventional mechanical and morphological responses [HB18]. It finds its application in stretchable electronics and in soft robotics. Kirigami structures can be easily elongated compared to the original sheets without cuts. This property make them behave like springs (see figure 4.7 and 4.8). Thus we incorporated a kirigami spring in our gripper design in order to get larger restoring torques about the output hinges.

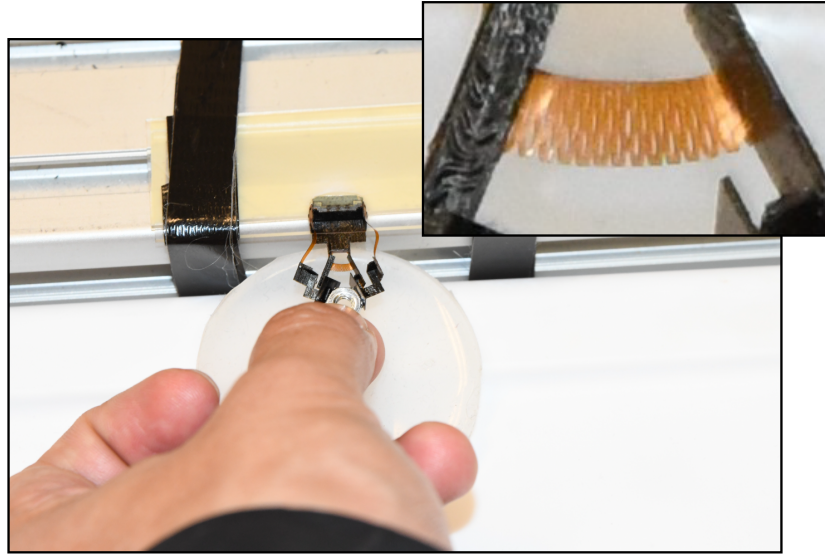


Figure 4.8: An image of the kirigami spring in action.

On loading of a kirigami spring, it initially undergoes a two-dimensional in-plane deformation, i.e. , stretching. In this regime it behaves as a hard, linear spring. On further loading there is a transition to an non-linear three-dimensional out-of-plane bending, when the in-plane deformation energy becomes equal to the out-of-plane deformation energy. In this regime it starts behaving like a soft, nonlinear spring. This transition results in the drop in the stiffness of the spring and as it no longer behaves like a linear-spring [IO16][TI19] it is difficult to find a model the stiffness of the kirigami spring. On further loading it enters the third regime where the deformation is rather localized near the tips of the cuts, leading to hardening of the mechanical response and finally to fracture.

Here we will assume that the kirigami spring to be hard and linear. This is for the simplicity of calculating the stiffness of the kirigami-spring which otherwise is non-linear. Nonetheless knowing the effective in-plane stiffness of the kirigami spring gives us the upper bound for the spring stiffness as the stiffness in the second regime is always lower.

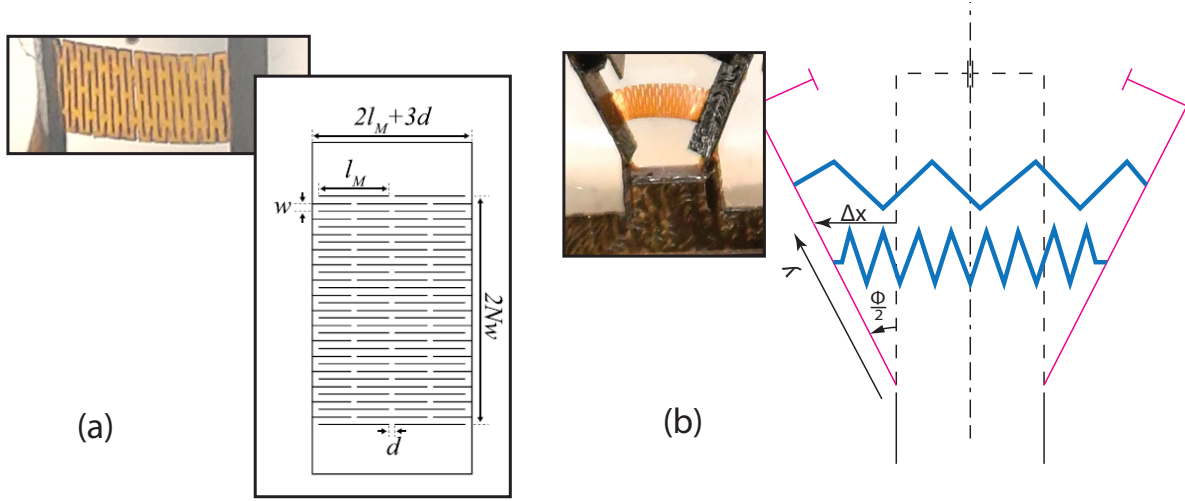


Figure 4.9: Figure(a) shows a schematic of a kirigami structure with geometric parameters. It is taken from [HB18], Figure 2(a). Figure (b) shows the variation in the elongation of the kirigami spring across its width.

The effective in-plane stiffness [HB18][IO16] of a kirigami structure can be calculated with the help of the equation:

$$\bar{K} = \alpha \frac{N_B}{N_{rows}} \frac{E w^3 t}{l_M^3} \quad (4.8)$$

where N_B is the number of beams in each row, N_{rows} is the number of rows along the loading direction, and α is a numerical coefficient which is dependent on boundary conditions and beam shape, E is the elastic modulus and l_M , w , and t are length, width, and thickness of the beam, respectively. The various design parameters involved in modeling of a kirigami spring is illustrated in the figure 4.9(a).

In order to determine the effective in-plane stiffness of the kirigami spring which has been incorporated in our modified gripper design, we need to know the kirigami design parameters. The value of the various design parameters of the kirigami spring, are $\alpha = 16$, $N_B = 2$, $N_{rows} = 25$, $E = 2.5 \text{ GPa}$, $w = 0.128 \text{ mm}$, $t = 0.0762 \text{ mm}$, $l_M = 0.625 \text{ mm}$. Plugging in these values in the equation 4.8, we get $\bar{K} = 2094.6 \text{ N/m}$.

From figure 4.9(b), it is evident that the deformation of the kirigami spring varies across

the width. The width of the kirigami is given by $2L_M + 2d$, which is $2 * 0.625 + 2 * 0.125 = 1.50 \text{ mm}$. (Notice the uncut regions at the ends are of length $d/2$, unlike the ones of length d as shown in the figure 4.9(a). Thus the width is NOT $2L_M + 3d$). As the width of the kirigami spring is small we can assume the displacement of the spring to be uniform and equal to the that at its mid-width i.e. $2\Delta x$.

$$2\Delta x = 2y \sin \frac{\phi}{2} = 2 \times (0.9 + 1.5/2) \sin \frac{\phi}{2} = 3.3 \sin \frac{\phi}{2} \text{ mm}$$

, where the distance of the kirigami structure from the output hinges is 0.9 mm and thus $y = 0.9 + 1.5/2 = 1.65 \text{ mm}$. Thereby we can obtain the approximate torque about the output hinge due to the elongation of the spring:

$$\tau_{sp} = \bar{K} \cdot 2\Delta x \cdot y = 0.0114 \sin \frac{\phi}{2} \text{ Nm}$$

Balancing moment about the output hinge,

$$F_{\text{output}} y_3 = \tau + \tau_{sp}$$

$$F_{\text{output}} = \frac{\tau + \tau_{sp}}{y_3} = \frac{1}{y_3} \left(k_{out} \frac{\phi}{2} + 0.0114 \sin \frac{\phi}{2} \right) = 0.058\phi + 1.485 \sin \frac{\phi}{2} \text{ N}$$

where y_3 needs to be converted to meters.

The plot in the figure 4.10(a) shows that the output force has been increased due to the incorporation of the kirigami spring in our gripper design.

The actuator force is given by:

$$F_{\text{actuator}} = \frac{\partial \left(\frac{1}{2} k_{in} (\theta)^2 + 2 \times \left(\frac{1}{2} k_{out} \left(\frac{\phi}{2} \right)^2 \right) + \frac{1}{2} \bar{K} (2\Delta x)^2 \right)}{\partial (r\theta)}$$

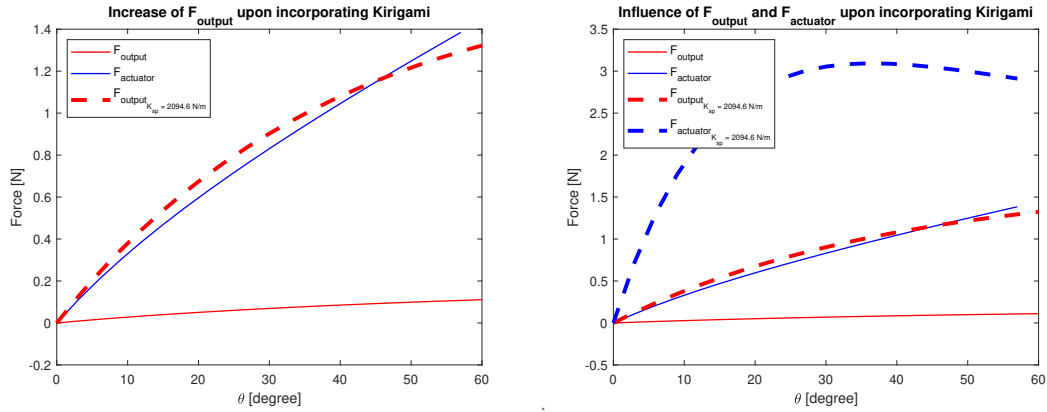


Figure 4.10: Influence of Kirigami spring on output force and on actuator force.

$$F_{actuator} = \frac{1}{r} (k_{in}\theta + k_{out} \frac{\phi}{2} \frac{\partial \phi}{\partial \theta} + \bar{K} (y \times 10^{-3}) \sin \phi \frac{\partial \phi}{\partial \theta}) \text{ N}$$

Clearly, the increase in the output force comes at the cost of increase in the actuator force, as depicted by the plot shown in the figure 4.10(b).

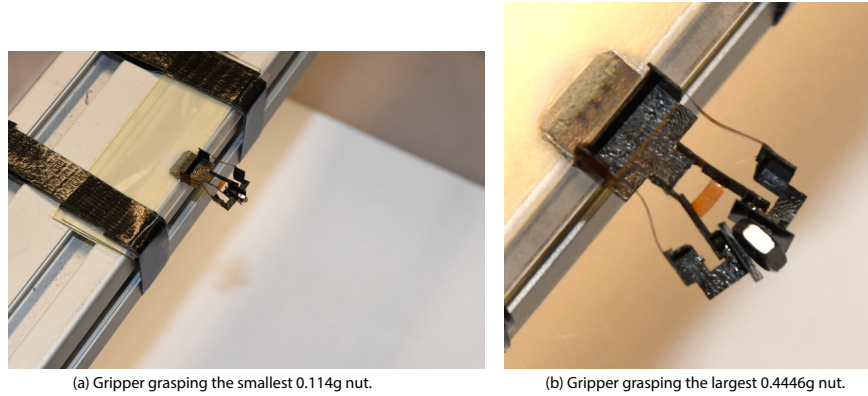


Figure 4.11: Images showing grasping of the target objects.

As a result of the incorporation of the kirigami spring-like structure, the gripper was able to establish a firm grip to the target hexagonal nuts (see figure 4.11).

Incorporating a kirigami structure in the design can be quite a challenging task. The top row of the figure 4.12 shows the modified version of the gripper in the making.

3. One way of reducing the actuator force can be by reducing the length of the input hinge. In

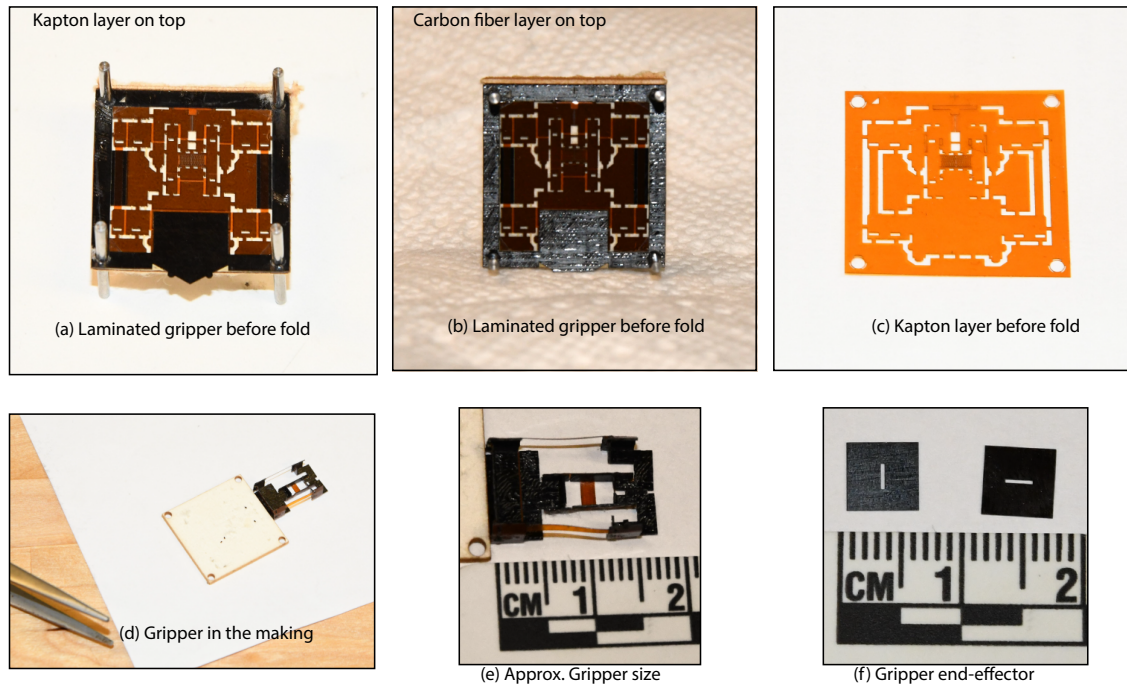


Figure 4.12: Some of the final images of the gripper.

the figure 4.13, the plot shows the extent to which the force for actuation can be lowered in our original design by making $x_1 = x_2$, where $x_2 = 2x_3$. However, this would also result in smaller lift of the object by the gripper as the input hinge stiffness is responsible for the lift.

4. The only component in the gripper design that is modular is the jaw tip or its end-effector (figure 4.12(f)). The coefficient of friction between the contact surfaces can be increased with the help of other available materials such as silicone, sand-paper etc.

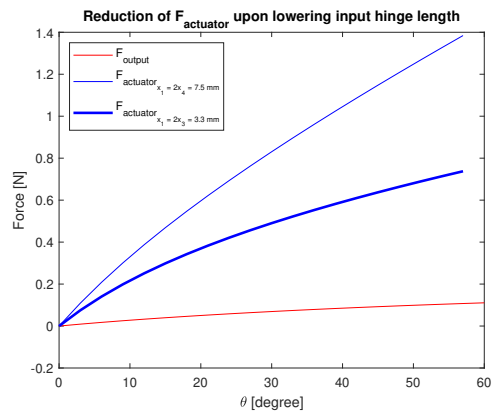


Figure 4.13: Influence of input hinge length on actuator force.

Chapter 5

Conclusion and Future Work

In micro-robotics one of the biggest challenges is the power source supply. In order to have an on-board power supply that can last for at least a couple of hours before recharging, it is critical to make use of power judiciously. This can be achieved through some smart designs. In this gripper design the gripper needs power only during picking the target object. Once it picks up the object, it needs no power and will be in its passive mode. Then the P3-robot would navigate at the desired location before finally powering up the gripper to place the object. Thus, this kind of pick-and-place gripper that would be passive for most of the time during its entire mission is desirable.

One limitation of this gripper design is that we do not have any control over the output force at the gripper tips once the gripper has been designed. So it is important to know how much force can the object withstand without being damaged. In our case study we were handling hexagonal nuts, thus it was strong enough to withstand large forces.

We still have some room for improvement of the gripper design in order to make it more robust, versatile and easy to build. Here are a few of the areas that can be worked on.

- In order to be versatile it needs to have adjustable end-effectors that could conform with the geometry of the target object. This can be achieved by adding some compliance to the

end-effector design.

- Due to a large range of applications, there is a lot of advancement in kirigami structure design and analysis. The work by Shyu *et al.* [SDD⁺15] shows how the different parameters associated with kirigami design prevent unpredictable local failure and increase the ultimate strain of the sheets. This is useful for a longer gripper lifetime. It is also shown that the sheets' tensile behaviour can be accurately predicted through finite-element modeling. This would help in conducting a more accurate analysis by taking into account of the non-linear stiffness of the kirigami spring as a result of three dimensional out-of-plane bending. There is also hybrid kirigami approach which reduces stiffness by a factor of 30 while increasing the ultimate strain by a factor of 2 [HB18]. It is worth exploring different kirigami patterns to identify which ones are more suitable for the micro-gripper based on the type of the target object.

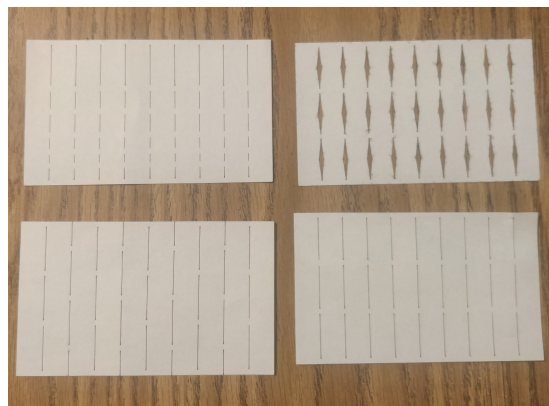


Figure 5.1: Some kirigami test patterns.

- We have seen that the entire micro-gripper, except the modular end-effectors, is built from a 2D laminate. The process of manually folding the 2D laminate into the 3D gripper is quite time-consuming and exhausting. We can take advantage of self folding shape-memory composites and integrate the method of self-folding hinges using shape memory polymers (SMPs) [FTS⁺13] [FTD⁺14] [TFM⁺14] [MYI⁺15].

The choice of actuator is the next crucial step for the entire project. Based on our gripper design, we see that we would need an actuator that can cause a displacement in the order of $r_{max} \frac{\pi}{6} = 2.078$ mm and can generate a minimum force of around 1.4 N in the case of the original micro-gripper or around 3.0 N in the case the modified kirigami-spring incorporated one. As per our application size, power consumption and cost needs to be minimized and hence the actuator must be selected accordingly. Even if the speed of the actuator is relatively slow, it should not be our main concern. The challenge is to incorporate the actuator within the limited space allotted on the P3 robot while being lightweighted.

Artificial muscle techniques can be used to actuate the microgripper. Thermal shape memory alloys (SMA) have very high work density (> 1 MJ/m³) and very high specific power (> 100 kW/kg) [MVA⁺04]. Thus it does not require a lot of space and does not increase the weight of the system significantly. Also, it has moderate strain (1-8%) and very high stress(200 MPa), which makes it suitable for our application. It is also readily available. The main drawbacks of SMA are they have low efficiency due to hysteresis, and are generally slow because of long response time and have short lifetime. Some of the other artificial muscles that are potential actuators for our application are dielectric elastomers and conducting polymers.

The paper [RI11] nicely elucidates the different kind of actuators that can be employed in micromanipulation , micrograsping tasks and their advantages and disadvantages. The most used piezoelectric materials are known for their high resolution, high speed, and high force density. SMA, on the other hand, have higher range of positioning (more than the hundred of micrometers) and of force (over ten of millinewton). However, SMA materials have a stronger nonlinearity than piezoelectric ones, making them hard to control. Electrothermal bimorph actuators also offers a large range of positioning (more than two hundreds of micrometers). However, it is more difficult to control the temperature of thermal actuators which often results a bad accuracy of the microgripper. In order to achieve both the high range and high resolution, the thermo-piezoelectric actuator is presented. As our microgripper design comes with the motivation of

saving power by making the grasping mode passive, it has a limitation. There cannot be any force control developed in our gripper, i.e. we cannot have any control over the output forces once the gripper has been designed. Only position control is possible with the help of the actuators. With thermo-piezoelectric actuator we can achieve position control of the gripper jaw tips. If we want to have a simpler system without any position control, SMAs are good candidate for our application.

This thesis is currently being prepared for submission for publication of the material.
Mondal, Sayan - The thesis author was the primary investigator and author of this material.

Bibliography

- [BYX⁺15] Joyce C Breger, ChangKyu Yoon, Rui Xiao, Hye Rin Kwag, Martha O Wang, John P Fisher, Thao D Nguyen, and David H Gracias. Self-folding thermo-magnetically responsive soft microgrippers. *ACS applied materials & interfaces*, 7(5):3398–3405, 2015.
- [DGS⁺15] N. Doshi, B. Goldberg, R. Sahai, N. Jafferis, D. Aukes, R. J. Wood, and J. A. Paulson. Model driven design for flexure-based microrobots. In *2015 IEEE/RSJ International Conference on Intelligent Robots and Systems (IROS)*, pages 4119–4126, 2015.
- [FTD⁺14] Samuel Felton, Michael Tolley, Erik Demaine, Daniela Rus, and Robert Wood. A method for building self-folding machines. *Science*, 345(6197):644–646, 2014.
- [FTS⁺13] Samuel M Felton, Michael T Tolley, ByungHyun Shin, Cagdas D Onal, Erik D Demaine, Daniela Rus, and Robert J Wood. Self-folding with shape memory composites. *Soft Matter*, 9(32):7688–7694, 2013.
- [GSR⁺18] P. Glick, S. A. Suresh, D. Ruffatto, M. Cutkosky, M. T. Tolley, and A. Parness. A soft robotic gripper with gecko-inspired adhesive. *IEEE Robotics and Automation Letters*, 3(2):903–910, 2018.
- [HB18] Doh-Gyu Hwang and Michael D Bartlett. Tunable mechanical metamaterials through hybrid kirigami structures. *Scientific reports*, 8(1):1–8, 2018.
- [HSB19] Paul WJ Henselmans, Gerwin Smit, and Paul Breedveld. Mechanical follow-the-leader motion of a hyper-redundant surgical instrument: Proof-of-concept prototype and first tests. *Proceedings of the Institution of Mechanical Engineers, Part H: Journal of Engineering in Medicine*, 233(11):1141–1150, 2019. PMID: 31526098.
- [IO16] Midori Isobe and Ko Okumura. Initial rigid response and softening transition of highly stretchable kirigami sheet materials. *Scientific reports*, 6:24758, 2016.
- [KKJ02] Manfred Kohl, Berthold Krevet, and Elmar Just. Sma microgripper system. *Sensors and Actuators A: Physical*, 97:646–652, 2002.
- [KPM92] C-J Kim, Albert P Pisano, and Richard S Muller. Silicon-processed overhanging microgripper. *Journal of Microelectromechanical Systems*, 1(1):31–36, 1992.

- [KPML90] C-J Kim, Albert P Pisano, Richard S Muller, and Martin G Lim. Polysilicon microgripper. In *IEEE 4th Technical Digest on Solid-State Sensor and Actuator Workshop*, pages 48–51. IEEE, 1990.
- [LRB⁺09] Timothy G Leong, Christina L Randall, Bryan R Benson, Noy Bassik, George M Stern, and David H Gracias. Tetherless thermobiochemically actuated microgrippers. *Proceedings of the National Academy of Sciences*, 106(3):703–708, 2009.
- [MVA⁺04] J. D. W. Madden, N. A. Vandesteeg, P. A. Anquetil, P. G. A. Madden, A. Takshi, R. Z. Pytel, S. R. Lafontaine, P. A. Wieringa, and I. W. Hunter. Artificial muscle technology: physical principles and naval prospects. *IEEE Journal of Oceanic Engineering*, 29(3):706–728, 2004.
- [MYI⁺15] Yiqi Mao, Kai Yu, Michael S Isakov, Jiangtao Wu, Martin L Dunn, and H Jerry Qi. Sequential self-folding structures by 3d printed digital shape memory polymers. *Scientific reports*, 5:13616, 2015.
- [NZ07] SK Nah and ZW Zhong. A microgripper using piezoelectric actuation for micro-object manipulation. *Sensors and Actuators A: Physical*, 133(1):218–224, 2007.
- [RI11] Micky Rakotondrabe and Ioan Alexandru Ivan. Development and force/position control of a new hybrid thermo-piezoelectric microgripper dedicated to micromanipulation tasks. *IEEE Transactions on Automation Science and Engineering*, 8(4):824–834, 2011.
- [RLB⁺08] Jatinder S Randhawa, Timothy G Leong, Noy Bassik, Bryan R Benson, Matthew T Jochmans, and David H Gracias. Pick-and-place using chemically actuated microgrippers. *Journal of the American Chemical Society*, 130(51):17238–17239, 2008.
- [SDD⁺15] Terry C Shyu, Pablo F Damasceno, Paul M Dodd, Aaron Lamoureux, Lizhi Xu, Matthew Shlian, Max Shtein, Sharon C Glotzer, and Nicholas A Kotov. A kirigami approach to engineering elasticity in nanocomposites through patterned defects. *Nature materials*, 14(8):785–789, 2015.
- [SJQ⁺19] Jessica A Sandoval, Saurabh Jadhav, Haocheng Quan, Dimitri D Deheyn, and Michael T Tolley. Reversible adhesion to rough surfaces both in and out of water, inspired by the clingfish suction disc. *Bioinspiration & Biomimetics*, 14(6):066016, oct 2019.
- [TFM⁺14] Michael T Tolley, Samuel M Felton, Shuhei Miyashita, Daniel Aukes, Daniela Rus, and Robert J Wood. Self-folding origami: shape memory composites activated by uniform heating. *Smart Materials and Structures*, 23(9):094006, 2014.
- [TI19] Hiroki Taniyama and Eiji Iwase. Design of rigidity and breaking strain for a kirigami structure with non-uniform deformed regions. *Micromachines*, 10(6):395, 2019.

- [Tri89] William SN Trimmer. Microrobots and micromechanical systems. *Sensors and actuators*, 19(3):267–287, 1989.
- [WAS⁺08] R. J. Wood, S. Avadhanula, R. Sahai, E. Steltz, and R. S. Fearing. Microrobot Design Using Fiber Reinforced Composites. *Journal of Mechanical Design*, 130(5), 03 2008. 052304.
- [WLT⁺16] F. Wang, C. Liang, Y. Tian, X. Zhao, and D. Zhang. Design and control of a compliant microgripper with a large amplification ratio for high-speed micro manipulation. *IEEE/ASME Transactions on Mechatronics*, 21(3):1262–1271, 2016.
- [ZG20] W Zhou and N Gravish. Soft microrobotic transmissions enable rapid ground-based locomotion. In *IROS*, 2020.
- [ZS09] Mohd Nashrul Mohd Zubir and Bijan Shirinzadeh. Development of a high precision flexure-based microgripper. *Precision Engineering*, 33(4):362–370, 2009.